A spatio-temporal nonlinear semi-analytical framework describing longitudinal waves propagation in damaged structures based on Green-Volterra formalism

Damien Bouvier, Marc Rébillat, Eric Monteiro, Nazih Mechbal

Arts et Métiers Institute of Technology, CNRS, CNAM, PIMM, HESAM Université, Paris, France

marc.rebillat@ensam.eu

December 19, 2022

Abstract

Structural Health Monitoring (SHM) of aeronautic structures by means of Lamb waves opens promising perspectives in terms of maintenance costs reduction and safety increases. Lamb waves interactions with damages are known to be nonlinear, a property still largely underexploited in SHM. Difficulties in this context are i) to be able to distinguish between nonlinearities due to the waves spatial propagation (i.e. material or geometrical nonlinearities) and those located at the damage position, ii) to handle computational complexity associated with spatio-temporal nonlinear models, and iii) to be able to physically link recorded signals with actual damage state. This work proposes to rely on the Green-Volterra formalism to build up a semi-analytical spatio-temporal framework describing longitudinal waves propagation and damage interaction able to physically represent both types of nonlinearities, and computationally simple enough to be tractable in real-time for SHM purposes. This approach is detailed here for longitudinal waves, which corresponds in the low frequency $\times$ thickness range to the S_0 Lamb wave mode propagating in a damaged beam. A spatio-temporal semi-analytical model of the nonlinear longitudinal waves propagation is first derived, where the damage is represented by a polynomial stiffness characteristic acting via boundary conditions at a given position in the beam. This model is then used to derive the Green-Volterra series describing the nonlinear input-output relationship of the system. A modal decomposition of the Green-Volterra series is also provided to ease implementation and reduce computational cost. The proposed spatio-temporal semi-analytical approach is then successfully compared to state-of-the-art nonlinear Lamb waves simulation methods based on finite-element models. It is finally shown on a simulated example and discussed in detail how such a nonlinear framework could potentially be relevant for SHM purposes.

1 Introduction and problem statement

Structural Health Monitoring (SHM) combines advanced sensor technology with intelligent algorithms in order to autonomously and in real-time interrogate the health condition of monitored structures. SHM applications are found in civil and mechanical engineering as well as in aerospace

and aeronautics where it can lead to large reduction of maintenance costs associated with great benefits in safety. Generally speaking, a SHM process entails establishing: (1) the existence of damage (detection step), (2) the damage location (localization step), (3) the type of damage (classification step), and (4) the damage severity (quantification step) [1–3].

The focus is put here on aerospace and aeronautic applications where structures to be monitored are aluminum or composite thin and large panels. In order to deploy SHM to such structures, Lamb waves are very appealing thanks to their long range propagation characteristics [4–6]. The underlying idea when monitoring structures by means of Lamb waves is to send such waves within the structures under study and to monitor echoes caused by potential damages apprearing in the structures. These echoes are then the basis of the damage detection, localization, classification and quantification steps that are usually carried out in a linear context (see for example [7–11]). This linear context assumes that the interaction between the incoming Lamb waves is linear in the temporal domain, *i.e.* that even if mode conversion can occur, there are no temporal nonlinear effects appearing during the Lamb wave damage interaction (such as higher harmonic generation or modulation effects for example). However, there are now numerous experimental proofs demonstrating that the Lamb wave/damage interaction is nonlinear and can thus generate higher harmonic or be responsible for modulation effects [12–20].

On the basis of the assumption that in many cases damage causes a structure to exhibit nonlinear dynamical response [21, 22] and that the SHM process can be significantly enhanced if one takes advantage of these nonlinear effects, several damage monitoring strategies have been proposed in the literature [23–25]. Starting from a linear framework, some authors [26–28] have shown that a nonlinear damage will impact the transmissibility functions (*i.e.* the frequency domain ratio between two different outputs of the system) and they used such information to detect and locate the damage. Extending the notion of transmissibility functions to nonlinear systems that can be described by Volterra series, Lang et. al [29, 30] were able to quantify the decrease of linearity generated by a nonlinear damage and thus to effectively detect and locate it. However, as such approaches are focusing on the loss of linearity, they do not seem to be able to deal with systems that are nonlinear in their healthy states, a fact that is quite common in real life. To overcome this drawback, several authors attempted to fit a nonlinear model (such as Volterra series [31]) to the nonlinear structure under study and to compare the actual and predicted outputs, or directly the model coefficients, under different damage conditions [32–40]. By doing so, they were able to detect numerically and experimentally a nonlinear damage even in an initially nonlinear structure, but not to take into account instrisic variablity caused by the environment and experimental noise. In order to tackle this issue, stochastic [41–43] and adaptive [44, 45] versions of Volterra series have been proposed for damage monitoring purposes. These methods are very encouraging but are all based on a single domain (either time or frequency) approach of the nonlinear damage monitoring problem and do not take into account its spatial dimension. Adding the spatial dimension to the above mentioned approaches, and more precisely to Volterra series [31], could however allow to:

1. naturally distinguish between nonlinearities due to the waves spatial propagation (i.e. material or geometrical nonlinearities) and those located at the damage position,

2. easily handle computational complexity associated with spatio-temporal nonlinear models,

3. draw a closer physical link between Lamb waves recorded signals and actual damage state as the nonlinear problem spatial dimension will be considered.

We thus aim here at providing a spatio-temporal framework with a richer semi-analytical representation of nonlinear damages and nonlinear propagation applied to Lamb waves propagation in composite or aluminum aeronautic complex structures. In order to model nonlinearities, this paper relies on the Volterra formalism [31]. Volterra series is a model representation that describes the output signal of a system as an homogeneous series with respect to the input [46]. This approach, similar to Taylor series approximations for functions, has been shown to be an universal approximator for any nonlinear dynamical system with fading memory [47]. To correctly take into account the spatial dependency of the problem under study, this paper uses the Green-Volterra series [48, 49], which are an extension of the Volterra formalism incorporating the notion of Green's function. Furthermore, we use the method presented in [49] which allows to easily compute the Green-Volterra kernels for an inhomogeneous nonlinear partial differential equation where the nonlinearities are put in a general polynomial form. In addition to the original work on that topic [48, 49], the inclusion of nonlinear boundary conditions and the derivation of solutions in the form of propagating waves are here achieved to reach that goal.

Furthermore, it should be noticed that Lamb waves are waves that are propagating in plate-like structures and waves that are by essence multimodal and dispersive [4–6, 50, 51]. In their lower frequency range, which is the one targeted by SHM application [8, 9], only two propagating modes exists. The first symmetrical mode, denoted as S_0 mode, mainly corresponds to *"longitudinal"* deformations and converges to longitudinal waves when the frequency tends toward zero. The first asymmetrical mode, denoted as A_0 mode, mainly corresponds to *"flexural"* deformations and converges to bending waves when the frequency tends toward zero. In practice, the S_0 mode is the one that propagates faster and thus often the easiest to use for damage monitoring in a SHM context [4, 5]. Furthermore, engineering structures to be monitored are mostly symmetrical with respect to their mid-plane and consequently the S_0 and A_0 mode are mathematically decoupled in such structures and can thus be studied independently from each other. Consequently, as a first approach to the full SHM problem, it has been chosen here to focus only on the S_0 mode in mono-dimensional structures by studying longitudinal waves propagating in nonlinear damaged beam-like structures.

In this paper, we thus use the Green-Volterra formalism to find spatio-temporal semi-analytical solutions for the longitudinal waves nonlinear propagation and nonlinear damage interaction in a damaged beam. Firstly, the longitudinal waves propagation model used for the damaged beam as well as the Green-Volterra formalism are presented in Section 2. Section 3 provides two spatio-temporal solutions for the damaged beam problem: one semi-analytical and one using a modal decomposition. Simulations are then presented in Section 4, and the proposed approach is sucessfully compared to a state-of-the-art method based on finite elements. Section 5 then presents a method for estimating the stiffness characteristic of the damage which corresponds to both the damage classification and damage size quantification steps of the SHM process. Finally, the proposed framework advantages and drawbacks are discussed in Section 6 and a conclusion is given in Section 7.

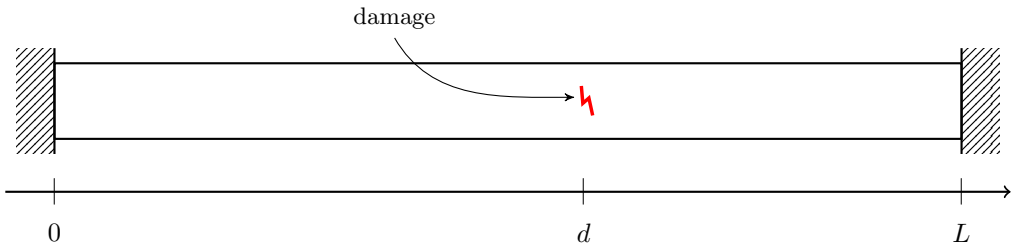

Figure 1: Damaged beam under study.

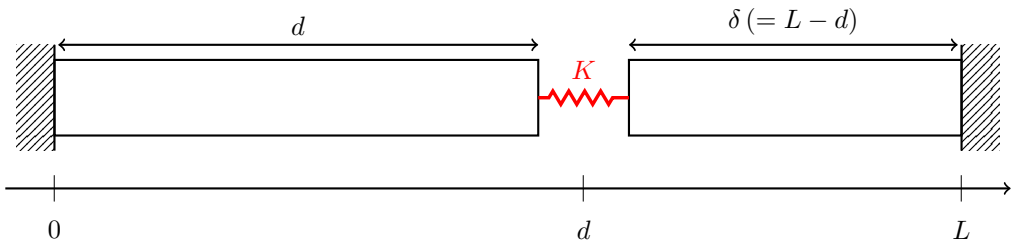

Figure 2: Simplified model used for approximating a damaged beam, using two sub-beams linked by a pointwise spring.

2 Longitudinal waves nonlinear propagation in a damaged beam

2.1 Modelling assumptions

As previously stated, the focus is put here on the longitudinal waves propagation within a nonlinear damaged beam. The longitudinal waves of a damaged beam under an external force $f(x,t)$ are denoted $u(x,t)$. We consider a beam of length L and section S, with fixed boundary conditions at both ends[1] and a damage localized at $x = d$ (see Fig. 1), and made of an homogeneous, isotropic and dissipative material, with Young modulus E, volumic mass ρ and damping factor γ. For sake of completeness, physical nonlinearity in the propagation is also taken into account, with ϵ and β respectively the quadratic and cubic nonlinearity coefficients [52].

The damage is represented as an infinitesimally small (i.e. pointwise) nonlinear spring linking two sub-beams, the left and right-part of the beam under study (see Fig. 2). This modelisation choice is purely theoretical, but seems reasonably adequate to the authors for some types of damages, e.g. a crack or a delamination that could open or close with the longitudinal waves, or a local change in material or geometrical properties leading to a localized variation in mechanical characteristics. Furthermore, SHM objective is to monitor damage premises, i.e. damages that in practice are small in comparison with monitored structures representative size, which is in agreement with the proposed approach.

In order to later use the Volterra formalism, we make the assumption that this nonlinear spring

[1]The presented approach is also valid for other types of boundary conditions, but for sake of clarity and concision we restrict here the presentation to this case only.

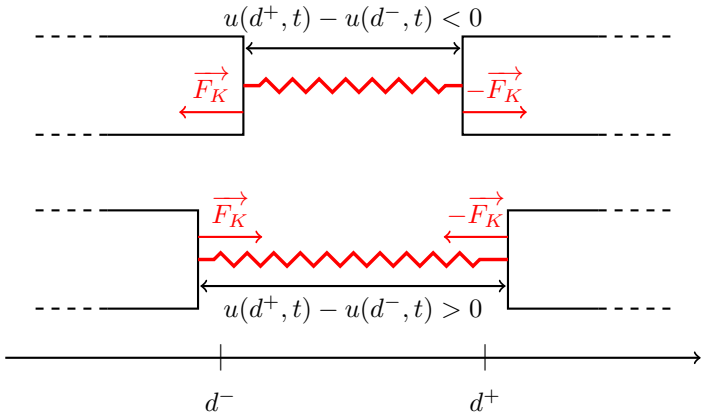

Figure 3: Representation of the restoring forces due to the spring acting on boundaries $x = d^-$ and $x = d^+$ in two different cases.

is characterized by a polynomial stiffness relation, i.e. the force $F_K[x]$ applied by the spring at its extremities in response to an elongation x is given in magnitude by:

$$F_K[x] = \sum_{n=1}^{+\infty} K_n x^n \,. \tag{1}$$

In the following, for simplicity, lets denote $f(d^-) = \lim_{x\to d, x\leq d} f(x)$ and $f(d^+) = \lim_{x\to d, x\geq d} f(x)$ for any space-dependent function f. The *"elongation"*[2] of the spring is thus given at all time t by $u(d^+,t) - u(d^-,t)$ (see Fig. 3). In the following, $\Omega_l = [0,d[$ and $\Omega_r =]d,L]$ will respectively denote the left-part and right-part domains, and $\delta = L - d$ the length of the right-part beam.

2.2 Constitutive equations

Given the previous assumptions, the longitudinal wave $u(x,t)$ follows the wave equation

$$\rho S\,\partial_t^2 u(x,t) + \gamma\,\partial_t u(x,t) - ES\left(1 - \epsilon\,\partial_x u(x,t) + \beta\,(\partial_x u(x,t))^2\right)\partial_x^2 u(x,t) = f(x,t) \tag{2}$$

for $x \in \Omega_l \cup \Omega_r$.
Furthermore, the fixed extremities at $x = 0$ and $x = L$ give the boundary conditions

$$u(0,t) = 0\,, \tag{3}$$
$$u(L,t) = 0\,, \tag{4}$$

and the damage imposes at boundaries $x = d^-$ and $x = d^+$ the conditions

$$ES\,\partial_x u(d^-,t) = F_K\left[u(d^+,t) - u(d^-,t)\right]\,, \tag{5}$$
$$-ES\,\partial_x u(d^+,t) = -F_K\left[u(d^+,t) - u(d^-,t)\right]\,. \tag{6}$$

[2]We will use the term *elongation* even if the spring is pointwise.

The constitutive equations describing the longitudinal waves propagation in the damaged beam model are thus given by

$$\Sigma : \begin{cases} \dfrac{1}{c_L^2}\partial_t^2 u\,(x,t) + \dfrac{\gamma}{F_0}\partial_t u\,(x,t) - \left(1 - \epsilon\,\partial_x u\,(x,t) + \beta\,\left(\partial_x u\,(x,t)\right)^2\right)\partial_x^2 u\,(x,t) = \dfrac{1}{F_0} f\,(x,t) \\ \qquad\qquad\qquad\qquad\qquad\qquad\qquad\qquad\qquad\qquad\qquad\qquad\qquad\qquad \text{for } x \in \Omega_l \cup \Omega_r \\ u\,(0,t) = 0 \\ u\,(L,t) = 0 \\ \partial_x u\,(d^-,t) = \partial_x u\,(d^+,t) = \partial_x u\,(d,t) \\ F_0\,\partial_x u\,(d,t) = F_K\left[u\,(d^+,t) - u\,(d^-,t)\right] \end{cases} \tag{7}$$

with $c_L = \sqrt{\frac{E}{\rho}}$ the longitudinal wave celerity, and $F_0 = ES$ a factor homogeneous to a force.

The longitudinal waves u is thus solution of a non-homogeneous differential equations system made up of one nonlinear propagation equation on $\Omega_l \cup \Omega_r$, two homogeneous Dirichlet boundary conditions at $x = 0$ and $x = L$, one homogeneous Cauchy boundary conditions at $x = d$ and one inhomogeneous Robin boundary conditions at $x = d$.

2.3 Volterra and Green-Volterra series

The Volterra series is an input-output system representation which has been used for many decades to model a variety of nonlinear dynamical systems [31, 46]. This model relies on the assumption that the output signal can be described, around an equilibrium, as an homogeneous series, i.e. that

$$u = \sum_{n=1}^{+\infty} u_n \tag{8}$$

where each output u_n is homogeneous of order n w.r.t. the input f, i.e. $u_n \propto f^n$.

For the readers not used to the Volterra formalism, the use of an homogeneous series approximation of a system is related to the principle of the Taylor series approximation of a function. This idea allows to extend the idea of linear filter to each order of nonlinearity via the introduction of Volterra kernels, which allows interesting frequency analysis of nonlinear phenomena [53, 54]. One important property of Volterra series is that it can approximate any nonlinear dynamical system with fading memory [47].

An extension of the Volterra formalism, the Green-Volterra series, has been introduced in [48, 49] to model problems that were also space-dependent. Furthermore, a method was proposed in [49] to easily compute these Green-Volterra series in the case of a partial differential equations of the form

$$\mathcal{L}_{x,t}[u](x,t) = f(x,t) + P\,[u]\,(x,t) \tag{9}$$

subject to linear boundary value conditions, where $\mathcal{L}_{x,t}$ is a linear space-time differential operator and P is a polynomial in u and its derivatives that regroups all nonlinearities of the problem. Using an approach similar to regular perturbation theory, the authors have shown that, in this case, each output u_n respects the following linear differential equations:

$$\mathcal{L}_{x,t}[u_1](x,t) = f(x,t)\,, \tag{10}$$

$$\mathcal{L}_{x,t}[u_n](x,t) = P_n\,[u_1, \ldots, u_{n-1}]\,(x,t) \text{ for } n \geq 2\,, \tag{11}$$

where P_n is a static combination of the u_m's and their derivatives, constructed from P (see [49, § 3.1] for more details about this calculation). Therefore, in order to represent and/or simulate Eq. (9), it is only needed to know and compute the Green kernel of the operator $\mathcal{L}_{x,t}$ with correct boundary conditions: this kernel encompasses all the dynamical part of the model, whereas nonlinearities are solely expressed in the P_n's (i.e. in the coefficients of P).

In the following, we will extend this approach to derive semi-analytical solutions for the longitudinal waves nonlinear propagation in a damaged beam stated in Eq. (7), where nonlinearities are also present in the boundary conditions. Small improvement with respect to [49] have been achieved as we extend the method to take into account also nonlinear boundary conditions and solutions in the form of propagating waves are provided.

2.4 Problem reformulation using Green-Volterra series

Following the approach used in [49], the model equations (7) can be reformulated

$$\Sigma : \begin{cases} \mathcal{L}_{x,t}[u]\left(x,t\right) = \dfrac{1}{F_0} f\left(x,t\right) + \left(-\epsilon\, \partial_x u\left(x,t\right) + \beta\, \left(\partial_x u\left(x,t\right)\right)^2\right) \partial_x^2 u\left(x,t\right) \quad \text{for } x \in \Omega_l \cup \Omega_r \\ u\left(0,t\right) = 0 \\ u\left(L,t\right) = 0 \\ \partial_x u\left(d^-,t\right) = \partial_x u\left(d^+,t\right) = \partial_x u\left(d,t\right) \\ \mathcal{D}_x[u]\left(t\right) = \sum_{n=2}^{+\infty} K_n \left(u\left(d^+,t\right) - u\left(d^-,t\right)\right)^n \end{cases} \tag{12}$$

with $\mathcal{L}_{x,t}$ the linear differential operator representing the wave propagation in the beam given by

$$\mathcal{L}_{x,t}[u]\left(x,t\right) = \frac{1}{c_L^2}\partial_t^2 u\left(x,t\right) + \frac{\gamma}{F_0}\partial_t u\left(x,t\right) - \partial_x^2 u\left(x,t\right) , \tag{13}$$

and $\mathcal{D}_x$ the linear part of the inhomogeneous Robin boundary condition at $x = d$ given by

$$\mathcal{D}_x[u]\left(t\right) = F_0\, \partial_x u\left(d,t\right) - K_1 u\left(d^+,t\right) + K_1 u\left(d^-,t\right) . \tag{14}$$

Let's now make the assumption that the output longitudinal waves can be written as an homogeneous series. In order to obtain constitutive equations for each order u_n, an approach similar to regular perturbation theory is used: the series form of Eq. (8) is incorporated in the Eq. (7), then terms are sorted and regrouped by homogeneity order (i.e. terms that are linear w.r.t. input f are grouped together, then those quadratic w.r.t. f, etc.) in order to give one sub-model for each homogeneity order n. This gives the following constitutive equations for each order n:

$$\Sigma_n : \begin{cases} \mathcal{L}_{x,t}[u_n]\left(x,t\right) = g_n\left(x,t\right) & \text{for } x \in \Omega_l \cup \Omega_r \\ u_n\left(0,t\right) = 0 \\ u_n\left(L,t\right) = 0 \\ \partial_x u_n\left(d^-,t\right) = \partial_x u_n\left(d^+,t\right) = \partial_x u_n\left(d,t\right) \\ \mathcal{D}_x[u_n]\left(t\right) = r_n\left(t\right) \end{cases} \tag{15}$$

with the "input force" g_n given by

$$g_1\left(x,t\right) = \frac{1}{F_0} f\left(x,t\right) \tag{16}$$

and, for $n \geq 2$,

$$\begin{aligned} g_n(x,t) = \epsilon & \sum_{\substack{m \in \mathbb{N}^2 \\ m_1+m_2=n}} \partial_x u_{m_1}(x,t)\, \partial_x^2 u_{m_2}(x,t) \\ & - \beta \sum_{\substack{m \in \mathbb{N}^3 \\ m_1+m_2+m_3=n}} \partial_x u_{m_1}(x,t)\, \partial_x u_{m_2}(x,t)\, \partial_x^2 u_{m_3}(x,t) \ , \end{aligned} \tag{17}$$

and the *"residual force"* r_n at damage given by

$$r_1(t) = 0 \tag{18}$$

and, for $n \geq 2$,

$$r_n(t) = \sum_{j=2}^{n} K_j \sum_{\substack{m \in \mathbb{N}^j \\ m_1+\cdots+m_j=n}} \prod_{k=1}^{j} \left(u_{m_k}(d^+,t) - u_{m_k}(d^-,t) \right). \tag{19}$$

From Eq. (15) and the expression of g_n and r_n, we can remark that each order u_n is the solution of a linear differential problem with mixed boundary conditions, where the *"input force"* and part of the boundary condition are function of lower orders u_m with $m < n$. Nonlinearities due to the propagation only appear in g_n for $n \geq 2$, whereas those due to the damage appears only in r_n for $n \geq 2$.

The analysis and resolution of the damaged beam problem for all orders n is equivalent to the study and analysis of operator $\mathcal{L}_{x,t}$ with corresponding boundary conditions. Furthermore, the resolution can be made iteratively, i.e. beginning at order $n = 1$ and going up until a truncation order N.

3 Spatio-temporal problem resolution

This section presents two different approaches for resolving constitutive equations (15). § 3.1 presents an semi-analytical solution in the Laplace domain, which allows frequency analysis but has limited possibilities for simulation purposes. § 3.2 presents an approximate solution using modal decomposition, which allows real-time simulation.

3.1 Semi-analytical solution in the Laplace domain

Consider the expression of (15) in the Laplace domain:

$$\Sigma_n : \begin{cases} \mathcal{L}_{x,s}[U_n](x,s) = G_n(x,s) & \text{for } x \in \Omega_l \cup \Omega_r \\ U_n(0,s) = 0 \\ U_n(L,s) = 0 \\ \partial_x U_n(d^-,s) = \partial_x U_n(d^+,s) = \partial_x U_n(d,s) \\ \mathcal{D}_x[U_n](s) = R_n(s) \end{cases} \tag{20}$$

with $\mathcal{L}_{x,s}$ the Laplace version of differential operator $\mathcal{L}_{x,t}$ given by

$$\mathcal{L}_{x,s}[U_n]\,(x,s) = \Big(\sigma(s)^2 - \partial_x^2\Big) U_n\,(x,s)\ ,$$

with

$$\sigma(s)^2 = \frac{s^2}{c_L^2} + \frac{\gamma s}{F_0}\,,$$

and where spatio-frequency signals U_n, G_n and R_n are the Laplace transform of spatio-temporal signal u_n, g_n and r_n. The dynamic part of the solution of (20), i.e. $\forall s \neq 0$, is given by (see Appendix A.1 for detailed computation)

$$U_n\,(x,s) = \begin{cases} \dfrac{K_1}{2\sigma(s)Q\,(s)} \displaystyle\int_0^L G_n(\xi,s)\Big(\cosh\Big(\sigma(s)(L-|x-\xi|)\Big) - \cosh\Big(\sigma(s)(L-x-\xi)\Big)\Big)\,d\xi \\ \quad + \dfrac{F_0\cosh\Big(\sigma(s)\delta\Big)}{2Q\,(s)} \displaystyle\int_0^d G_n(\xi,s)\Big(\sinh\Big(\sigma(s)(d-|x-\xi|)\Big) - \sinh\Big(\sigma(s)(d-x-\xi)\Big)\Big)\,d\xi & \text{for } x\in\Omega_l\,, \\ \quad + \dfrac{R_n\,(s)}{Q\,(s)}\cosh\Big(\sigma(s)\delta\Big)\sinh\Big(\sigma(s)x\Big) \\ \dfrac{K_1}{2\sigma(s)Q\,(s)} \displaystyle\int_0^L G_n(\xi,s)\Big(\cosh\Big(\sigma(s)(L-|x-\xi|)\Big) - \cosh\Big(\sigma(s)(L-x-\xi)\Big)\Big)\,d\xi \\ \quad + \dfrac{F_0\cosh\Big(\sigma(s)d\Big)}{2Q\,(s)} \displaystyle\int_d^L G_n(\xi,s)\Big(\sinh\Big(\sigma(s)(\delta-|x-\xi|)\Big) + \sinh\Big(\sigma(s)(L+d-x-\xi)\Big)\Big)\,d\xi & \text{for } x\in\Omega_r\,, \\ \quad - \dfrac{R_n\,(s)}{Q\,(s)}\cosh\Big(\sigma(s)d\Big)\sinh\Big(\sigma(s)\,(L-x)\Big) \end{cases} \tag{21}$$

where

$$Q\,(s) = K_1\sinh\Big(\sigma(s)L\Big) + F_0\,\sigma(s)\cosh\Big(\sigma(s)\delta\Big)\cosh\Big(\sigma(s)d\Big)\,. \tag{22}$$

The static part, i.e. for $s = 0$, is given by (see Appendix A.2 for detailed computation)

$$U_n(x,0) = \begin{cases} \dfrac{K_1 L}{F_0 + K_1 L} \displaystyle\int_0^L G_n(\xi,0)\left(\mathbb{1}_{[0,x]}(\xi)\,\xi + \mathbb{1}_{[x,L]}(\xi)\,x - \frac{\xi x}{L}\right) d\xi \\ \quad + \dfrac{F_0}{F_0 + K_1 L} \displaystyle\int_0^d G_n(\xi,0)\left(\mathbb{1}_{[0,x]}(\xi)\,\xi + \mathbb{1}_{[x,d]}(\xi)\,x\right) \qquad \text{for } x \in \Omega_l\,, \\ \quad + \dfrac{x}{F_0 + K_1 L} R_n(0) \\ \dfrac{K_1 L}{F_0 + K_1 L} \displaystyle\int_0^L G_n(\xi,0)\left(\mathbb{1}_{[0,x]}(\xi)\,\xi + \mathbb{1}_{[x,L]}(\xi)\,x - \frac{\xi x}{L}\right) d\xi \\ \quad + \dfrac{F_0}{F_0 + K_1 L} \displaystyle\int_d^L G_n(\xi,0)\left(L - \mathbb{1}_{[d,x]}(\xi)\,x - \mathbb{1}_{[x,L]}(\xi)\,\xi\right) d\xi \qquad \text{for } x \in \Omega_r\,. \\ \quad - \dfrac{(L-x)}{F_0 + K_1 L} R_n(0) \end{cases} \tag{23}$$

Left and right part in Eq. (21) share the same first term, which is, to a factor, the longitudinal waves of a healthy beam of length L fixed at both its boundaries. For the left part (respectively the right part), the second term is, also to a factor, the longitudinal waves of an healthy beam of length d (resp. $\delta = L - d$) with fixed-free boundary condition (resp. free-fixed). In both parts, the third and last term corresponds to the longitudinal waves induced by the inhomogeneous Robin boundary condition due to the damage.

Furthermore, if $K_1 = +\infty$ (i.e. the damage acts as a non deformable link between both left and right parts), we recover perfectly the case of a fixed-fixed healthy beam of length L. For the linear term U_1, if we consider $K_1 = 0$ (i.e. the damage does not link both parts), we recover perfectly the equations for two separate healthy beams. The same remarks can be made for the static solution provided in Eq. (23).

In order to use equations (21−23) for numerical simulation, it will be necessary to perform a numerical Fourier transform and its inverse. Therefore damping is needed, otherwise discretization of the frequency domain will cause leaking effects that prevent simulating the transient response[3]. This also impedes the simulation from being computed in real-time.

Furthermore, spatial integral appears in Eq. (21−23), which will introduce numerical approximations. One possible workaround is to only consider point-wise excitation force, i.e. of the form $\delta(x - x_0)\,F(s)$; but even when considering this special type of input, and when nonlinear propagation terms are taken into account (i.e. when $\epsilon \neq 0$ and $\beta \neq 0$), pseudo-input force G_n for $n \geq 2$ will not be point-wise, and the problem of numerical spatial integral remains (if the propagation is linear, then G_n for $n \geq 2$ are always zero).

To alleviate those requirements, the next section presents a modal decomposition that can be practically used to solve Eq. (15).

[3]Stationnary response for sinusoidal excitation would still be computable, but a large majority of works in the SHM domain are interested in transient responses.

3.2 Approximate solution using a modal decomposition

Because the model described by Eq. (15) is a linear problem (w.r.t. g_n and r_n), it can be decomposed onto an orthonormal basis. § 3.2.1 introduces the modal decomposition used, and § 3.2.2 presents how it is used to compute approximate solutions of Eq. (15).

3.2.1 Modal shapes

For the p^{th} mode, depending whether the damage is positioned on an anti-node or not, its modal shape ϕ_p can be of one of two forms (see Appendix B.1 for detailed computations).

General case: Consider first the case where the damage is not positioned on an anti-node (which is the more general case), i.e. $\phi_p'(d) \neq 0$. Therefore the modal shape ϕ_p has a discontinuity at $x = d$, and its shape is given by

$$\phi_p(x) = \begin{cases} A_p \sin(\lambda_p x) & \text{for } x \in \Omega_l\,, \\ -A_p \dfrac{\cos \lambda_p d}{\cos \lambda_p \delta} \sin\Big(\lambda_p (L - x)\Big) & \text{for } x \in \Omega_r\,, \end{cases} \tag{24}$$

with

$$A_p = \sqrt{\frac{2\cos(\lambda_p\delta)^2}{d\cos(\lambda_p\delta)^2\Big(1 - \operatorname{sinc}(2\lambda_p d)\Big) + \delta\cos(\lambda_p d)^2\Big(1 - \operatorname{sinc}(2\lambda_p\delta)\Big)}}\,, \tag{25}$$

and where the wavenumber λ_p is the p^{th} solution of the transcendental equation

$$0 = \frac{F_0}{K_1} + \frac{\operatorname{sinc}(\lambda d)}{\cos(\lambda d)} + \frac{\operatorname{sinc}(\lambda\delta)}{\cos(\lambda\delta)}\,. \tag{26}$$

Particular case: If the damage is exactly on an anti-node, i.e. $\phi_p'(d) = 0$, the modal shape is continuous and analogous to a modal shape of a healthy beam of length L. This type of modal shape is quite rare, and appears only if there exists $(n, m) \in \mathbb{N}^2$ such that

$$\frac{(n + 1/2)\,\pi}{d} = \frac{(m + 1/2)\,\pi}{\delta}\,. \tag{27}$$

Its shape is then given by

$$\phi_p(x) = \sqrt{\frac{2}{L}} \sin\left(\frac{(n + m + 1/2)\,\pi}{L} x\right). \tag{28}$$

Figure 4 shows the first modal shapes for a damaged beam. All modes are quite similar in shape to those of an healthy beam with fixed boundary conditions at both its extremities, except for the discontinuity at the damage position; the fifth mode, which is a particular case where the damage position corresponds exactly to the fourth anti-node, is exactly equal to the corresponding healthy mode.

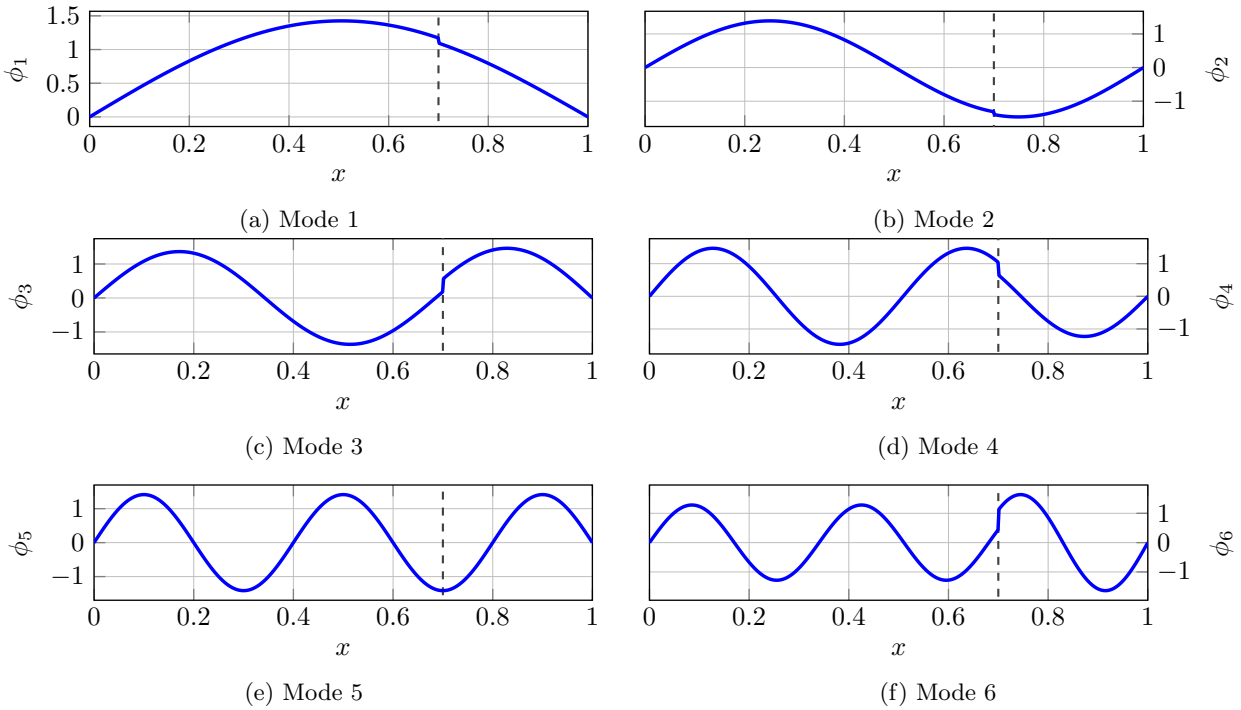

(a) Mode 1 (b) Mode 2

(c) Mode 3 (d) Mode 4

(e) Mode 5 (f) Mode 6

Figure 4: The first six modal shapes for a damaged beam (with $L = 1$ m, $F_0 = 2.1 \cdot 10^7$ N, $d = 0.7$ m and $K_1 = 0.7 \cdot 10^9$ N/m); the fifth one is a particular case, where the damage position corresponds to the fourth anti-node.

3.2.2 Modal solution

The modal solution of problem (15) is given by (see Appendix B.3 for detailed computations)

$$u_n(x,t) = h(x)\, r_n(t) + \sum_{p=1}^{+\infty} \phi_p(x)\, u_{n,p}(t) \ , \tag{29}$$

where h is a spatial shape with null second derivative, added to take into account the inhomogeneous boundary condition $\mathcal{D}_x[u_n](t) = r_n(t)$, given by

$$h(x) = \begin{cases} \dfrac{x}{F_0 + K_1 L} & \text{for } x \in \Omega_l \ , \\ -\dfrac{(L-x)}{F_0 + K_1 L} & \text{for } x \in \Omega_r \ , \end{cases} \tag{30}$$

and where $u_{n,p}$ is the temporal evolution of the p-th mode, which follows the ordinary differential equation

$$\ddot{u}_{n,p}(t) + \frac{c_L^2 \gamma}{F_0} \dot{u}_{n,p}(t) + \lambda_p^2 c_L^2 u_{n,p}(t) = c_L^2 \langle g_n, \phi_p \rangle(t) - \langle h, \phi_p \rangle \Big(\frac{c_L^2 \gamma}{F_0} \dot{r}_n(t) + \ddot{r}_n(t) \Big) \ , \tag{31}$$

where the notation $\langle a, b \rangle$ corresponds to the spatial scalar product between a and b, i.e.

$$\langle a, b \rangle = \int_0^L a(x) b(x) d\,x\,. \tag{32}$$

The modal solution of (15) can thus be numerically simulated, for each order n, as follows:

1. compute terms g_n and r_n from previous orders u_m, $m < n$ (for $n = 1$, we have $g_1(x,t) = f(x,t)$ and $r_1(t) = 0$);
2. compute derivatives $\dot{r}_n$ and $\ddot{r}_n$ via numerical derivation;
3. compute factors $\langle h, \phi_p \rangle$ using Eq. (83) and (84);
4. compute signals $\langle g_n, \phi_p \rangle (t)$ either using a numerical integral, or using an analytical approach similar as the one in §4.3 in [49];
5. numerically solve Eq. (31) using any discretization method (Euler method, bilinear transform, first-order hold, etc);
6. compute the solution using Eq. (29).

Using the modal approach, there are no restrictions on the damping of the system nor on the input signal (its modal decomposition must either be known in advance or computed using numerical integrals). Furthermore, this approach could be carried in real-time, if proper precomputation is done for all the necessary terms.

4 Simulation benchmark comparison of the proposed longitudinal waves nonlinear propagation in a damaged beam

In this section, we will compare results provided by the two solutions of the damaged beam problem obtained from Eq. (7) (given in § 3.1 and § 3.2) with the same structure simulated by means of the SDTools Matlab Toolbox [55], a state-of-the-art analysis and simulation toolbox for dynamical analysis which uses the finite element method (FEM). The objectives of this section are to study the accuracy and computational efficiency of the proposed semi-analytical spatio-temporal solutions.

4.1 Simulation parameters

The base model is a steel beam of length $L = 1$ m, with a rectangular section of 20 mm by 5 mm (so a surface $S = 1\ \mathrm{cm}^2$), a Young modulus of $E = 210.0$ GPa, a density of $\rho = 7850.0$, $\mathrm{kg/m}^3$, and a damping factor of $\gamma = 5.0 \cdot 10^3\ \mathrm{kgm}^{-1}\mathrm{s}^{-1}$. For the simulation, the propagation is supposed linear, i.e. $\epsilon = 0$ and $\beta = 0$.
The damage is taken as a cubic spring, i.e. with a characteristic relation given by

$$F_K\,[x] = K_1 x + K_3 x^3\,, \tag{33}$$

where $K_1 = 0.7 \cdot 10^9$ N/m and $K_3 = 5.0 \cdot 10^{27}$ N/m^3. It is placed at $d = 0.7$ m.
The input force is taken as sine burst excitation, located at $x_0 = 0.3$ m. It is comprised of three cycles at $f_0 = 100$ kHz multiplied by a Hann window of unit amplitude, sampled at $f_s = 5$ MHz (see Figure 5). Output longitudinal waves are simulated for a duration of 1 ms and with a time step of 5×10^{-7} s .

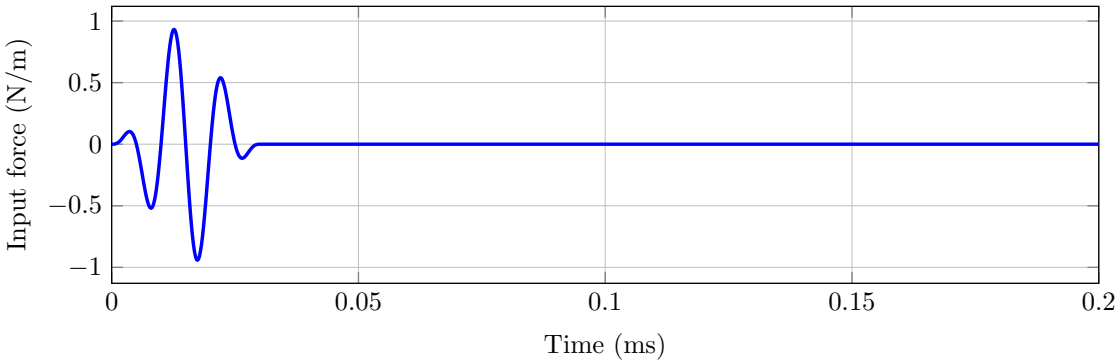

(a) Time representation

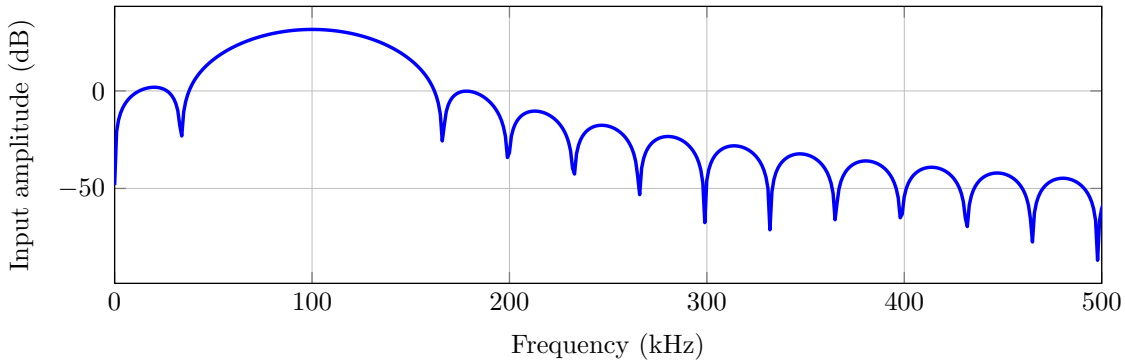

(b) Frequency representation

Figure 5: Input force signal used for the simulation in (a) time domain and (b) frequency domain representations.

Simulation method	Truncation order		
	$N = 7$	$N = 15$	$N = 25$
Semi-analytical solution	14.1dB	14.1dB	14.1dB
Modal solution (50 modes)	11.8dB	11.8dB	11.8dB
Modal solution (100 modes)	14.1dB	14.1dB	14.1dB

Table 1: RMS value (in dB) of the difference between the FEM results provided by SDTools and proposed methods for different truncation order N of the Green-Volterra series

For the finite-element model, the elements that are used are standard Bernoulli-Euler beam elements (12 DOF) based on linear interpolation for traction and torsion and cubic interpolation for flexion. The solver that is used is a Newmark implicit time integration method with $\gamma_N = 0.5$ and $\beta_N = 0.25$ (providing an unconditionally stable scheme). The beam was meshed with elements having a size of 1 mm resulting in a model containing 1000 elements and 1001 nodes.

For both simulation methods presented in this paper, only the $N = 15$ first orders of the series are simulated. This truncation order was selected so that precision brought by adding higher-order terms would be negligible (the 15^{th} order is more than 60dB below the first order in terms of amplitude). The semi-analytical solution simulation uses a zero-padding of 50000 points to avoid leaking effects in the Fourier and inverse-Fourier transform. This was selected to ensure that the longitudinal waves would be totally damped at the end of the analysis window. The modal solution simulation uses a number of 100 modes and a first-order hold as discretization method. The number of modes was chosen in order to represent a large enough dynamic range without being too costly to compute.

4.2 Simulation results

Figure 6 shows the space-time representation of the longitudinal waves simulated using the two proposed methods and the FEM simulation. We can see that obtained results are qualitatively similar for all three simulations. This can be further observed in Figure 7 which shows the first reflections at three positions (between the left boundary and the excitation at $x_1 = 0.15$m, between the excitation and the damage at $x_3 = 0.5$m, and between the damage and the right boundary at $x_3 = 0.85$m). It demonstrates that the proposed modelisation and simulations correctly reproduce the longitudinal waves in the temporal domain.
It can also be seen that the damage acts as a nonlinear semi-reflecting barrier, which creates harmonic distortion. These distortions are visible in the output spectra, shown in Figure 8 at the same three positions. It can be seen that the proposed simulations correctly reproduce the nonlinear dynamical behavior. The error observed above 250kHz in the modal approach is due to the number of modes used: more modes are needed to represent dynamics for higher frequencies, but it would impact the computation time. Furthermore, we can quantitatively compare simulations by computing the RMS value of their difference; those results are given in Table 1, which gives:

- a value of -14dB between the semi-analytical approach and the result given by SDTools;
- a value of -14dB between the modal approach and the result given by SDTools;

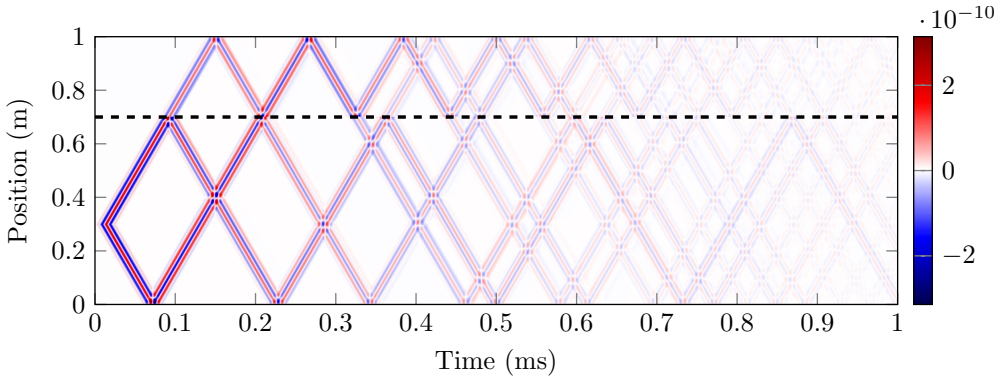

(a) Semi-analytical solution

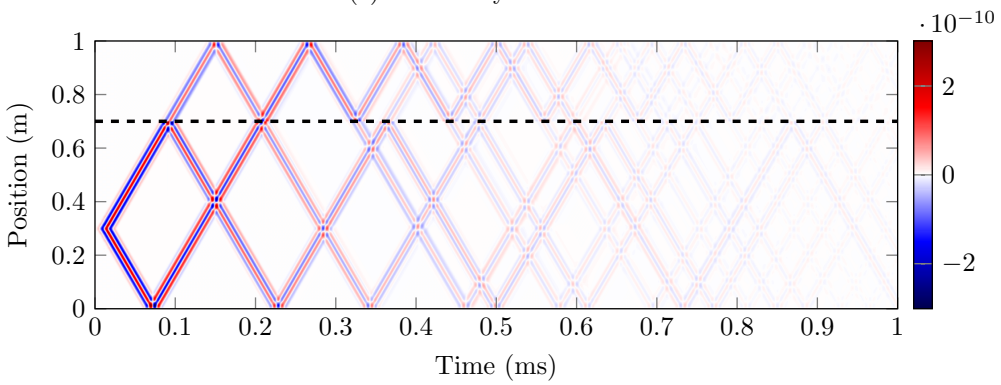

(b) Modal solution

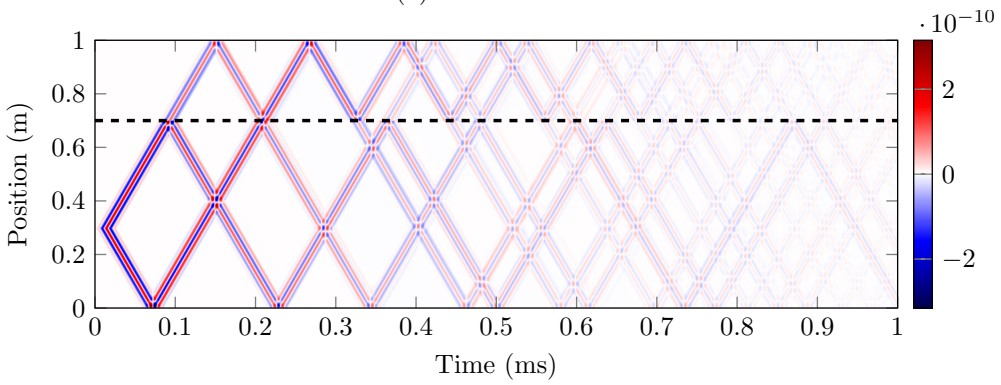

(c) FEM simulation

Figure 6: Space-time plot of the damaged beam using (a) the semi-analytical solution (see § 3.1), (b) the modal solution (see § 3.2), (c) a FEM toolbox available for Matlab; simulations parameters are presented in § 4.1.

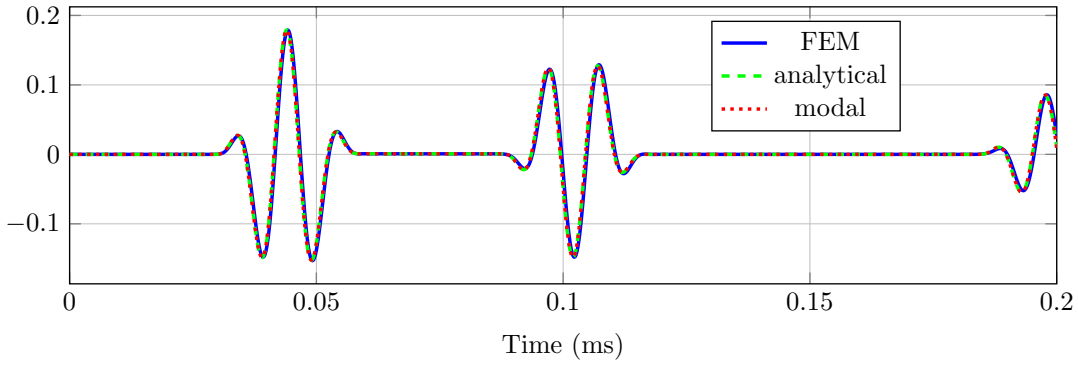

(a) $x_1 = 0.15$m

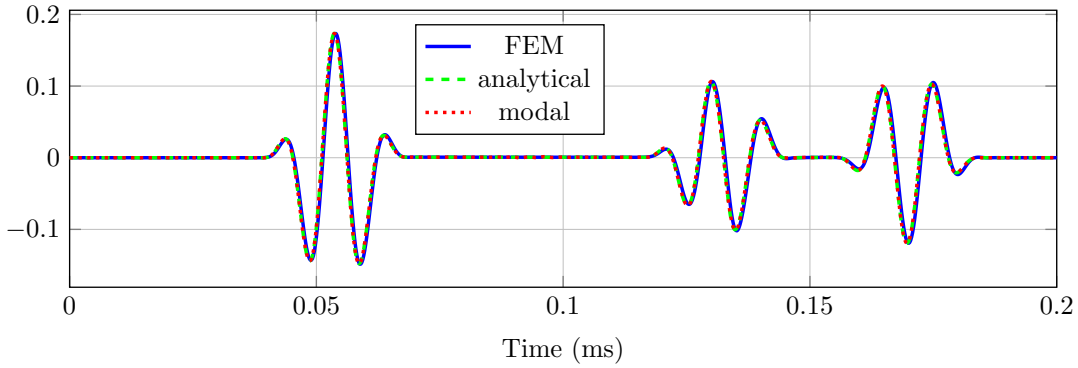

(b) $x_2 = 0.5$m

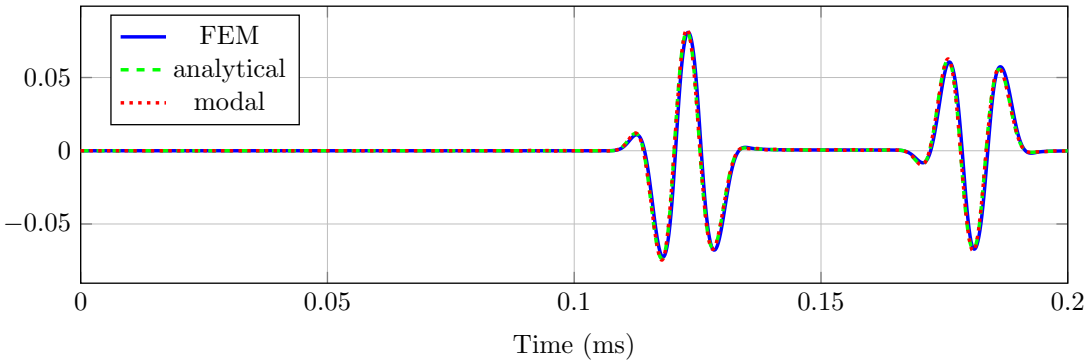

(c) At $x_3 = 0.85$m

Figure 7: First reflections of the longitudinal waves of the beam at three positions: (a) between the left boundary and the excitation at $x_1 = 0.15$m, (b) between the excitation and the damage at $x_3 = 0.5$m, (c) between the damage and the right boundary at $x_3 = 0.85$m; simulations parameters are presented in § 4.1.

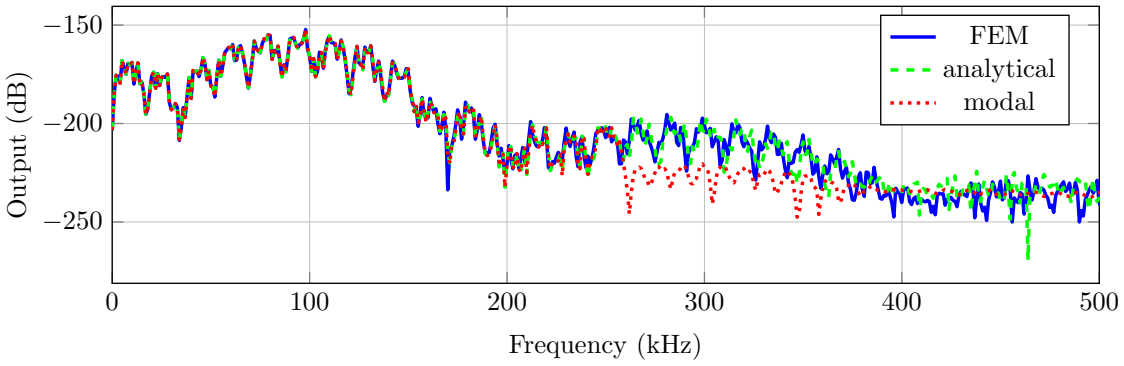

(a) $x_1 = 0.15$m

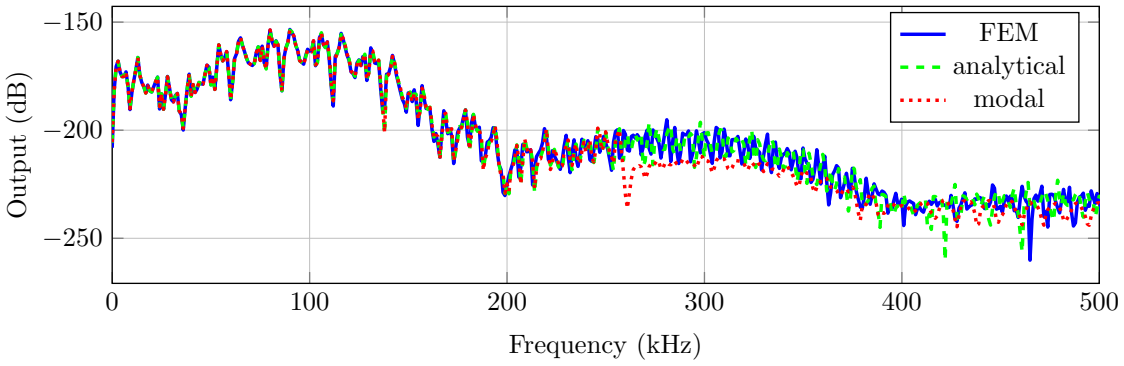

(b) $x_2 = 0.5$m

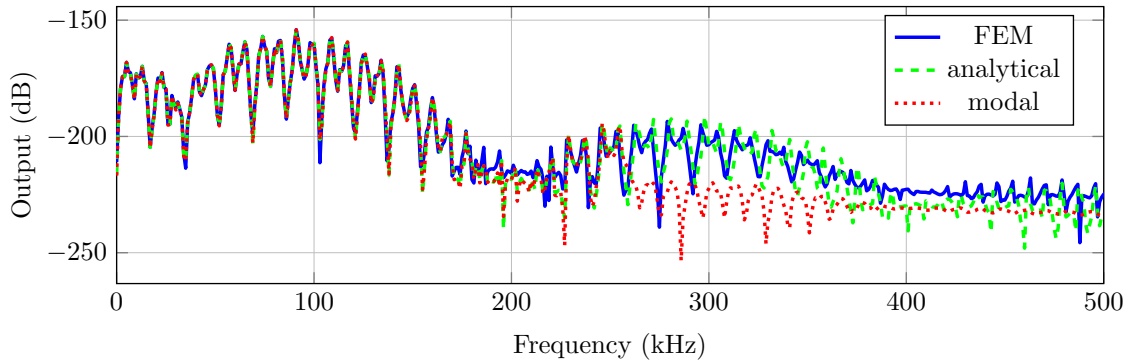

(c) At $x_3 = 0.85$m

Figure 8: Amplitude spectrum of the longitudinal waves of the beam at three positions: (a) between the left boundary and the excitation at $x_1 = 0.15$m, (b) between the excitation and the damage at $x_3 = 0.5$m, (c) between the damage and the right boundary at $x_3 = 0.85$m; simulations parameters are presented in § 4.1.

Simulation method	Complete discretization			SHM-like discretization		
	$N = 7$	$N = 15$	$N = 25$	$N = 7$	$N = 15$	$N = 25$
FEM	49.62s			~~49.62s~~		
Semi-analytical solution	139.12s	251.37s	446.63s	1.38s	3.17s	4.75s
Modal solution (50 modes)	70.97s	119.36s	214.03s	17.56s	37.97s	56.03s
Modal solution (100 modes)	148.37s	257.27s	446.16s	37.13s	70.27s	116.30s

Table 2: Computation time of the three simulation methods for different truncation order N of the Green-Volterra series; column *"Complete discretization"* corresponds to the spatial discretization used for the FEM simulation, here using 1001 equally spaced points; column *"SHM-like discretization"* corresponds to computing the longitudinal waves only for some position (corresponding to sensors in a SHM framework), here considering three sensors at $x_1 = 0.15$m, $x_2 = 0.5$m and $x_3 = 0.85$m.

- a value of -37dB between the modal and semi-analytical approach.

Therefore, the simulations using both proposed approaches and through SDTools obtain qualitatively and quantitatively similar results, thus validating the approach.

Table 2 shows the computation time of the three simulation methods in different cases; computations were made on a personal laptop with dual core 2.40GHz processors and 8 gigabytes of RAM. When the beam is represented using 1001 equally spaced points (left-column of the table), the FEM approach is significantly faster than the two proposed methods (between 2 to 10 times). But one advantage of the proposed methods is that it is possible to compute longitudinal waves only at specified points, which can be interesting in a SHM framework (where only longitudinal waves at sensors location is needed). In this case (right-column of the table), the two proposed methods can be significantly faster than a FEM approach, depending on method used and its parameters. Nonetheless, these comparisons have to be taken with precautions due to the fact that the FEM simulation used a highly-optimized and efficient Matlab Toolbox, whereas the proposed simulation methods were implemented in Python, and were not optimized for computation efficiency. Furthermore, it should be noted that the mesh size of the FEM is certainly too fine and can be coarsened without loosing accuracy. Another point is that high order elements combined with an explicit solver could also have been more efficient. This would result in a decrease of computational time. For both proposed simulation methods, the computation time grows almost linearly with the truncation order N; therefore, it is interesting to compute only the orders needed for a given wanted precision, i.e. to avoid computing orders that do not contribute significantly to the output longitudinal waves. Furthermore, the semi-analytical solution approach is much faster than the modal one when few points are needed, but this difference diminishes (or is even inverted) for a large number of spatial points. This can be explained by the fact that, in the modal approach, most of the computation is due to the numerical resolution of the ordinary differential equation (31) (which only depends on time and not on space), whereas in the semi-analytical approach most of the computation is due to the computation of output spectra from (21) and (23) (which are space dependent). Finally, we can observe that the computation time of modal simulation evolves almost linearly with the number of modes; therefore, if no precision is wanted in the high frequency domain, the number of modes can be kept quite low to reduce the computation time.

5 Damage parameters estimation

5.1 SHM context and underlying assumptions

SHM rely on smart-structures instrumented by sensors and actuators (piezo-electric elements for example) that can be considered as local [2,3,5]. Then, the damage monitoring process is classically performed in four steps:

1. Detection : is there a damage?
2. Localization : where is the damage?
3. Classification : what kind of damage is it?
4. Quantification : how large is the damage?

Damage detection is a topic that has been largely addressed using nonlinear approaches in the literature [26–28, 32–45]. The damage localization problem has been solved using linear based approaches [7, 9, 11] as well as using nonlinear based approaches [29, 30]. Consequently, we assume here that the damage has already been detected and localized and that the objective is now to classify it and to estimate its severity.

Consequently, this section presents a method for estimating the damage class and severity, i.e. the values of the coefficients K_n for n up to an chosen order N, in the case where all other parameters of the problem (geometry and material properties of the beam, and the position of the damage) are known, or can be estimated with good accuracy. The polynomial shape will provide information for damage classification whereas the polynomial coefficients values will be useful for damage quantification purposes. We will consider the case of a linear propagation (i.e. ϵ and β are null, or equivalently g_n is always null for $n \geq 2$). Furthermore, we will assume that the input force can be controlled and is a pointwise excitation located in x_i (i.e. $f(x,t) = \delta(x - x_i)f(t)$), and that longitudinal wave was measured in a location x_o. As previously stated, those assumptions correspond to the ones classicaly made in a SHM framework. First the method is presented in § 5.2, then its potential applicability to SHM for classification and quantification purposes is illustrated on a simulated system in § 5.3.

5.2 Estimation method

General idea

From Eq. (19), it can be seen that the residual force r_n at the damage depends only on the coefficients K_m with $m \leq n$. Therefore, access to output orders u_n would allow an iterative estimation procedure, i.e. estimate K_1 from u_1, then estimate K_2 from u_2 using the previously estimated K_1, etc. Fortunately, it is possible to extract output orders u_n from measurements using order separation methods such as described in [56–58].
The proposed method can be separated in three main steps:

1. separate orders u_n using the approach presented in § 4.2 of [58];
2. estimate K_1 from u_1 by fitting transfer functions;
3. for each $n = 1, \ldots, N$, estimate K_n from u_n using a least-squares approach.

These last two steps are now detailed.

Estimation of K_1

First the transfer function $\widetilde{H}$ is estimated using input F and the first separated order u_1, i.e.

$$\widetilde{H}\left(j2\pi f_k\right) = \frac{U_1\left(x_o, j2\pi f_k\right)}{F\left(x_i, j2\pi f_k\right)}\,. \tag{34}$$

Then coefficient K_1 is estimated by minimizing the following criteria (e.g. using a gradient descent method):

$$K_1 = \arg\min 10\log\left(\sum_{f_k}\left(\widetilde{H}\left(j2\pi f_k\right) - H\left(j2\pi f_k\right)\right)^2\right)\,, \tag{35}$$

where the true transfer function H is computed using (21) and (23), with $G_1(s) = F(s)/F_0$ and $R_1(s) = 0$.

Estimation of K_n, $n \geq 2$

The expression of the residual force r_n, given by equation (19), can be rewritten

$$r_n\left(t\right) = r_n^{\text{old}}\left(t\right) + r_n^{\text{new}}\left(t\right)\,, \tag{36}$$

with r_n^{old} the part of the residual force that only depends on coefficients K_m with $m < n$, given by

$$r_n^{\text{old}}\left(t\right) = \sum_{j=2}^{n-1} K_j \sum_{\substack{m\in\mathbb{N}^j \\ m_1+\cdots+m_j=n}} \prod_{k=1}^{j}\left(u_{m_k}\left(d^+, t\right) - u_{m_k}\left(d^-, t\right)\right), \tag{37}$$

and r_n^{new} the part of the residual force that depends only on the coefficient K_n to estimate, given by

$$r_n^{\text{new}}\left(t\right) = K_n\left(u_1\left(d^+, t\right) - u_1\left(d^-, t\right)\right)^n\,. \tag{38}$$

Because we have no propagation nonlinearities (i.e. G_n si null), we can see from (21) and (23) that the output longitudinal waves of order n linearly depends on r_n. We can thus define u_n^{old} (respectively u_n^{new}) in a similar fashion as for r_n^{old} (resp. r_n^{new}), i.e. the part of the order u_n that only depends on coefficients K_m with $m < n$ (resp. on coefficient K_n). We can then write

$$U_n\left(x,s\right) - U_n^{\text{old}}\left(x,s\right) = \begin{cases} \dfrac{R_n^{\text{new}}\left(s\right)}{Q\left(s\right)}\cosh\Big(\sigma(s)\delta\Big)\sinh\Big(\sigma(s)x\Big) \\ -\dfrac{R_n^{\text{new}}\left(s\right)}{Q\left(s\right)}\cosh\Big(\sigma(s)d\Big)\sinh\Big(\sigma(s)\left(L-x\right)\Big) \end{cases} \tag{39}$$

$$U_n\left(x,0\right) - U_n^{\text{old}}\left(x,0\right) = \begin{cases} \dfrac{x}{F_0 + K_1 L}R_n^{\text{new}}\left(0\right) \\ -\dfrac{\left(L-x\right)}{F_0 + K_1 L}R_n^{\text{new}}\left(0\right) \end{cases} \tag{40}$$

Because R_n^{new} linearly depends on K_n, so does $U_n\left(x,s\right) - U_n^{\text{old}}\left(x,s\right)$. It is therefore possible to estimate K_n using the following approach:

1. compute $U_n^{\text{old}}\left(x,s\right)$ using previously estimated coefficients;
2. compute the right-hand part of (39) and (40) taking $K_n = 1$;
3. estimate K_n using a least-square method between left and right-hand parts of (39) and (40).

5.3 Estimation results

In this section, the estimation method is tested on the same beam as described in § 4.1. Longitudinal wave responses are simulated using the FEM Matlab Toolbox SDTools, and the method is tested on three different output positions x_o: one at $x_1 = 0.15$m between the left boundary and the excitation , one at $x_2 = 0.3$m between the excitation and the damage, and the last at $x_3 = 0.85$m between the damage and the right boundary. The $N = 9$ first order are separated using the method presented in § 4.2 of [58], and then the 9 first coefficients K_n are estimated using the method described previously (see § 5.2).

Figure 9 shows the estimation result for the three output position and for different cases of added noise. The grey area corresponds to the region of excitation of the damage during the longitudinal waves propagation, i.e. values given outside this area are extrapolated from the estimated coefficients but this part of the characteristic was not at play during the longitudinal waves propagation. The problem encountered here is that a given nonlinear black box model, and by the way any black box model, cannot be correctly identified out of its excitation range [59]. This can be interpreted as an intrinsic inability of the estimated model to predict things out of the training range. We can however see that, in the non-extrapolated region, the damage characteristic is well estimated for any output data used; outside this region, the estimated characteristic can quickly diverge from the true value if there is noise present. In noisy environment (SNR = 20dB), the estimation begins to differ from the true value except for the output position $x_o = 0.85$m; this could be explained by the fact that, because the damage is situated in between this point and the excitation (which is at $x_i = 0.3$m), the impact of the damage on the propagation is greater than for the other two points (which are on the same side of the beam than the excitation).

In order to test how the estimation method can give an idea of the damage severity, we have repeated the previous experiment but with different cubic coefficient K_3 for the damage characteristic

$$F_K[x] = K_1 x + K_3 x^3 . \tag{41}$$

Figure 10 shows the estimation results for three different values of K_3. We can observe that, in the non-extrapolated region, the damage characteristic is well estimated for any damage severity and for any output position used. The modification of the polynomial coefficients of Eq. (41) can be interpreted from a SHM point of view as a modification of the damage severity (the more severe the damage is, the more nonlinear it will be). This numerical experiment thus illustrates how the proposed estimation can thus potentially be used for damage quantification purposes.

In the SHM community, damage is generally represented using various models like dry friction, coulomb friction, mechanical slack or bilinear relation (even if it has not been experimentally proven that these models are more realistic than polynomials). Figure 11 shows the estimation result for a damage with a dry friction characteristic. We can observe that this type of damage is not correctly estimated, even for the central linear part. This can be explained by the fact that the estimation method relies heavily on polynomial approximation, which can not correctly represent the discontinuities present in the dry friction characteristic. However, some useful information can still be extracted from these estimation results. For example, the shape of the estimated polynomial approximation may be representative of a given damage type and thus may be helpful for damage classification tasks.

Therefore we have shown that, in the case of a damage following a polynomial relation, the proposed estimation method can robustly estimate the damage characteristic in the displacement range where it has been excited and that these extracted characteristics potentially convey useful information for damage classification and quantification.

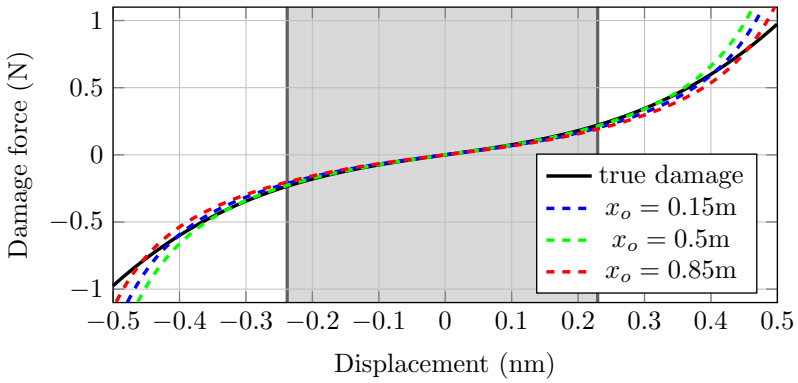

(a) Clean data

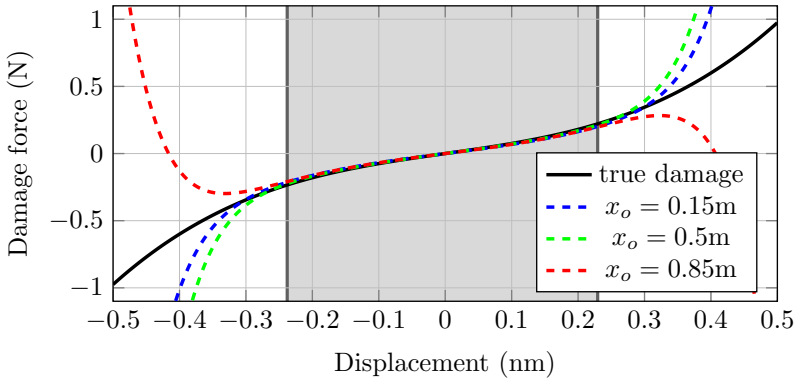

(b) SNR = 40dB

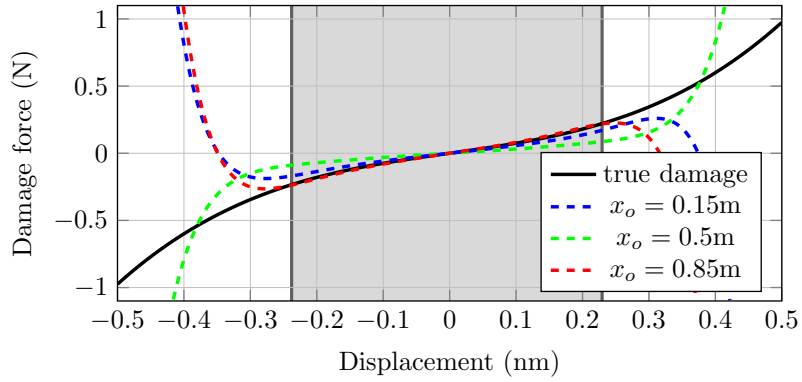

(c) SNR = 20dB

Figure 9: Damage characteristic and its estimation for different SNR and different output position x_o; the grey area corresponds to the region of excitation of the damage during the longitudinal waves propagation.

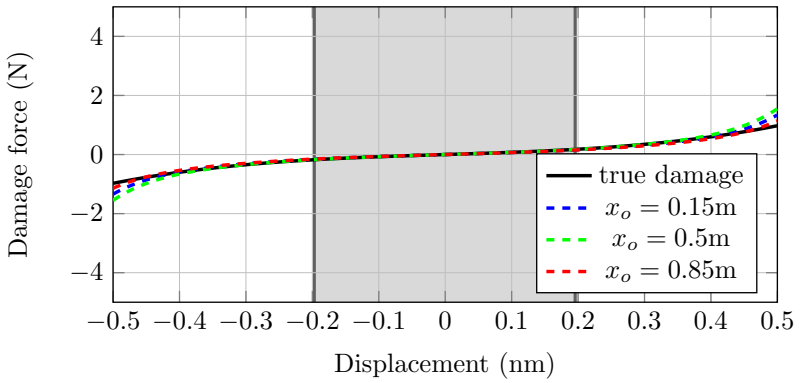

(a) $K_3 = 5.0 \cdot 10^{27}$ N/m^3.

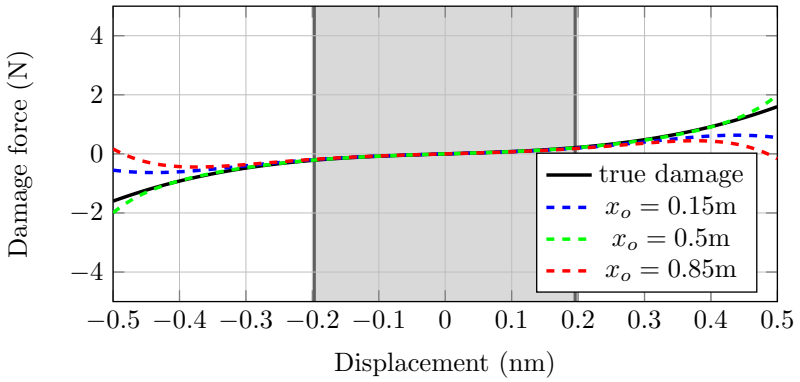

(b) $K_3 = 1.0 \cdot 10^{28}$ N/m^3.

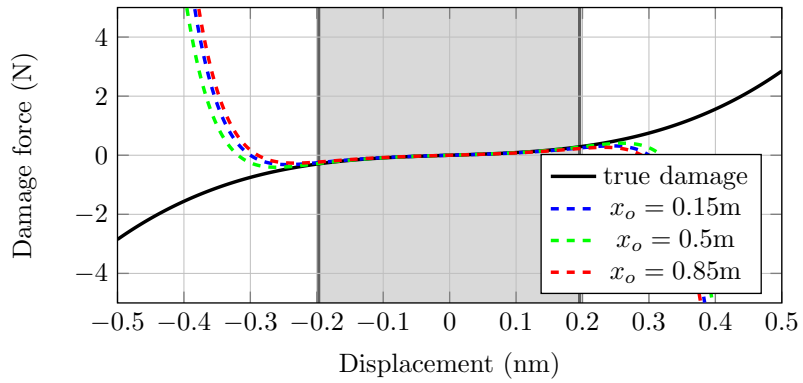

(c) $K_3 = 2.0 \cdot 10^{28}$ N/m^3.

Figure 10: Damage characteristic and its estimation for different damage severity (characterised by the cubic coefficient K_3) and different output position x_o; the grey area corresponds to the region of excitation of the damage during the longitudinal waves propagation.

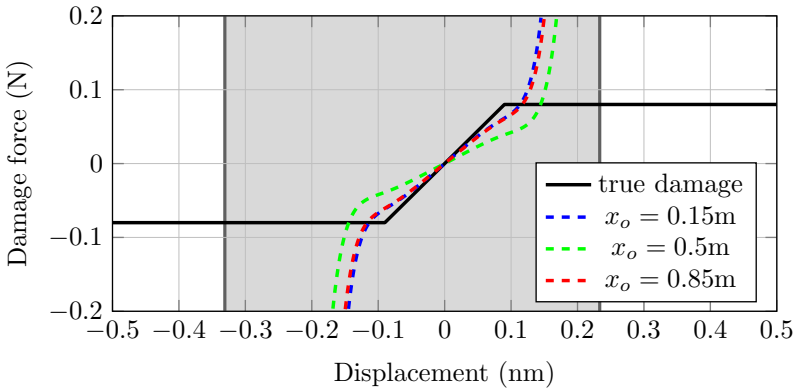

Figure 11: Damage characteristic and its estimation for different output positions x_o and with different SNR; the gray area corresponds to the region of excitation of the damage during the longitudinal waves propagation.

6 Discussion

The advantages and drawbacks of the proposed framework for longitudinal waves nonlinear propagation in a damaged beam, particularly with respect to its practical value for SHM purposes, are discussed in this section.

6.1 Modeling wave damage interaction using polynomial decompositions

One of the first concerns that can be raised considering the framework proposed here is that it fully relies on the assumption that the wave/damage interaction can be modeled using a polynomial approximation. This section aims at discussing why this is a reasonable choice both from an applicative and theoretical points of view, even if it is not representative of all the damage cases that can be encountered in practice and of all the existing nonlinear mathematical functions.

The practical objective is here to provide a tool for SHM purposes where the goal is to monitor damage evolution in an engineering structure at its earliest stage [2, 60]. Consequently, it is expected in practice that the framework summarized by Eq. (7), and more particularly the fact that the wave/damage interaction expressed as a polynomial approximation in Eq. (1), are indeed representative of structures containing damage at an early state. More precisely, the underlying idea is to monitor the dynamical nonlinearitites generated by the wave/damage interaction as they are expected to be extremely sensitive to the damage [23–25]. Physically, one can reasonably infer that small damages or damages at their earliest stage may dynamically behave relatively smoothly, and that their behavior will become more and more nonlinear as damages are growing up. As a consequence, if the focus is put only on the beginning of the damage evolution process, it can be admitted that from a physical perspective the polynomial approximation is sufficient with respect to the applicative purpose pursued here.

This question can also be considered from a theoretical point of view. Indeed, it has been mathematically demonstrated that polynomial developments can approximate any *"weakly"* nonlinear function [61, 62]. The vocabulary being used here, more precisely the word *"weakly"*, is a bit mis-

leading as it implicitly suggests that it is not a *"strong"* nonlinearity. However, mathematically, *"weakly"* here means that the function to be approximated should be continuous enough and does not tell how linear or not it should be. For example *exponential* and *arctan* functions are truly nonlinear but extremely continuous and thus can be extremely well approximated by polynomials. Furthermore the functions under study only need to be approximated locally and not through their whole definition domain (see Figures 9, 10, and 11 for example) which is also an argument in favor of polynomial expansions. Functions that are not continuous enough, as shown in Fig. 11 for the dry friction case which cannot be differentiated at two points, may however hardly be approximated in practice by such an assumption. Consequently, polynomial expansions appear here as a mathematical tool general enough to model a wide variety of nonlinear continuous functions and thus seems sufficient in practice here.

Another point of interest is related with the nonlinearities induced by the material itself that have been considered in the theoretical approach but not in the estimation procedure. The estimation method that was indeed proposed here made the assumption that the propagation is linear. If the nonlinear propagation parameters ϵ and β are known for the material and geometry under study, the proposed approach could easily be improved to incorporate nonlinear propagation. This would mean that, in the third step of the estimation process (i.e. the iterative estimation of the nonlinear damage coefficients), the part due to propagation would have to be included in r_n^{old}. If the nonlinear propagation parameters are unknown, they would then need to be estimated along the damage coefficient, which would surely impact the estimation robustness.

6.2 From mono-dimensional beams to bi-dimensional plates

A second concern that can be raised regarding the semi-analytical framework proposed here is that it targets mono-dimensional wave propagation. In real life applications, engineering structures to monitor can indeed be mono-dimensional (such as beam-like structures, structures build up of many beams, etc ...) but can also be bi-dimensional (like aeronautic composite or aluminum structures for example). An important question is thus if, and how, this framework can handle or be adapted to handle bi-dimensional structures.

As a first way to deal with this concern, one can notice that in practical SHM cases dealing with aeronautic composite or aluminum structure, the considered wavelengths are of the order of few *cm* to monitor meter scale structures [5, 6, 8–11]. In practice, even if those waves are being generated by a point-like source, this means that propagation can be considered as plane wave propagation. Furthermore, the attenuation of such waves is dominated by material attenuation [63] and thus the mono-dimensional plane wave equations can be considered to hold. Following that approach, even if the structures within which the waves propagate are 2D, a 1D propagation model thought as a ray tracing approach can be considered [64]. Consequently, the semi-analytical approach proposed in Sec. 3.1 can be used in a straightforward manner to address such a problem. However, the modal one that relies on beam modes and presented in Sec. 3.2 cannot be used as modes are not clearly defined in such a context. The ray-tracing approach may thus be a practical solution to reduce the 2D wave propagation problem related to SHM of composite aeronautic structure to a 1D one that suits the framework proposed here. An important issue regarding such an approach is however that wave/damage interaction would be poorly described as it remains a punctual interaction. An advantage of such an approach is that it will be computationally cheap.

In order to extend to 2D the proposed 1D framework, an alternate idea could be to entirely re-formulate the problem in a cylindrical coordinates system centered on the damage himself. The

problem at hand could thus be considered as axisymetric and 1D solutions can be found by relying on Hankel functions instead of exponential functions as elementary solutions of the linear problem. This approach is very common when addressing linear diffraction of Lamb waves by cylindrical obstacles [65–67]. Adapting the proposed framework on the basis of this idea may be complicated to manage in practice but seems however affordable from an analytical point of view. In order to simplify analytical computations, Hankel functions can furthermore by approximated by exponential functions after a few wavelengths, which could help. Such an approach to reduce the 2D problem to a 1D one seems more suitable from a physical point of view that the ray tracing approach but may lead to more analytical and computational complexities.

6.3 From longitudinal waves to S_0 and A_0 Lamb wave modes

A third concern is that SHM relies on Lamb waves and not on longitudinal waves as in the proposed framework. Lamb waves are waves that propagate in plate-like structures and are multimodal and dispersive [4–6, 50, 51]. In their lower frequency range, which is the one targeted by SHM application [8, 9], only two propagating modes exists. The first symmetrical mode, denoted as S_0 mode, mainly corresponds to *"traction/compression"* deformations and converges to longitudinal waves when the frequency tends toward zero. The first asymmetrical mode, denoted as A_0 mode, mainly corresponds to *"flexural"* deformations and converges to bending waves when the frequency tends toward zero. Furthermore, engineering structures to be monitored are mostly symmetrical with respect to their mid-plane and consequently the S_0 and A_0 mode are mathematically decoupled in such structures and can thus be studied independently from each other. This section will thus discuss if the proposed framework can be thought as representative of S_0 mode Lamb waves, how it could be adapted to be representative for A_0 mode Lamb waves, and point out one of its limitation which is that it is unable to represent mode conversion.

In practice, the S_0 mode is the one that propagates faster and thus often the easiest to use for damage monitoring in a SHM context [4, 5]. Consequently, as a first approach to the full SHM problem, this is why it has been chosen here to focus only on the S_0 mode in mono-dimensional structures by studying longitudinal waves propagating in nonlinear damaged beam-like structures. In that sense, the proposed framework can be thought as representative of the S_0 mode propagation.

The extension of the proposed framework to A_0 mode, i.e. to *"flexural"* waves can also be discussed. What is representative of longitudinal waves in the proposed formulation is the longitudinal wave equation provided by Eq. (2). In order to extend the proposed framework to the A_0 mode, it is thus simply necessary to replace this equation describing longitudinal waves by an equation describing flexural waves propagation like Eq. (42) [68] and to follow the same solutions derivation procedure as for the longitudinal case. Furthermore, boundary conditions (3) and damage conditions (5) also have to be replaced by corresponding relations for bending waves.

$$\rho S\,\partial_t^2 u\left(x,t\right)+\gamma\,\partial_t u\left(x,t\right)-\frac{ESh^3}{12(1-\nu^2)}\left(1-\epsilon\,\partial_x u\left(x,t\right)+\beta\,\left(\partial_x u\left(x,t\right)\right)^2\right)\partial_x^4 u\left(x,t\right)=f\left(x,t\right)\quad(42)$$

for $x\in\Omega_l\cup\Omega_r$ and with h the thickness and ν the material Poisson ratio.

It is also important to notice that the proposed framework is only able to represent part of the physical phenomenon happening during wave damage interaction. Indeed, when a S_0 mode Lamb wave interacts with a damage, the reflected and transmitted waves are not only S_0 mode Lamb waves but can also be of the A_0 mode type [4–6]. This phenomenon is known as mode conversion and is not handled by the framework proposed here. Indeed, one assumption retained here is that

S_0 and A_0 modes are decoupled from each other as a result of the symmetry of the structure with respect to its mid-plane. This assumption is true excepting at the damage location where mode conversion can occur and thus where S_0 and A_0 modes can be coupled. However, with respect to practical application this is not a major drawback. Indeed, care is often taken to make sure that the selected piezoelectric element diameters, geometry and input frequency ensures that one mode is dominant over the other one [50]. Consequently, even if mode conversion exists, it is not a major source of perturbation in practice and thus the proposed framework can still be considered as representative of what happens physically.

6.4 Framework exploitation for SHM purposes

Finally it can be discussed how this framework can be considered as useful for the SHM community. At least two points related to this can be mentioned and are developed in this section.

The first point is linked with the fact that finite-element simulation of both the nonlinear wave propagation and the nonlinear wave/damage interaction is something that is extremely hard to handle in practice. Usually authors from the literature either perform finite element simulations of nonlinear damages interrogated by waves propagating in a linear medium (see [15] or [18] for example) or analytical computations of waves propagating in a nonlinear undamaged medium (see for example [16] or [52]). To the authors knowledge, there are no published work allowing to simulate both nonlinear wave propagation and nonlinear wave/damage interaction. The proposed framework can by definition handle simultaneously those two effects at low computational costs. However, due to its semi-analytical formulation, the allowed geometries are very restricted. Consequently it can be very useful for the SHM community as a preliminary tool to benchmark nonlinear damage monitoring algorithms in the presence of nonlinear propagation and for example to assess whether nonlinear propagating phenomenon can be isolated from nonlinear wave/damage interaction by those algorithms.

From an applicative perspective, having low-cost and reliable numerical models offers other opportunities for the SHM community. Indeed, the main difficulties in SHM are to get data in damage states and to train or validate SHM algorithms [69]. Using the proposed framework, it is thus possible to get a better physical understanding of the nonlinear wave/damage interaction (which is actually in practice very poor as damages are very often modeled as density losses [8,9,70]) and thus expect to be able to better test and tune upcoming damage monitoring algorithms by benefiting of such an understanding. Furthermore, the actual tendency is to rely on machine learning algorithms fed by meta-models or low-cost simulation models for SHM purposes [71, 72]. The proposed framework also appears as a good candidate to generate data-sets allowing to train and validate such algorithms.

7 Conclusion

In this study, we have shown how the Green-Volterra formalism can be used to find spatio-temporal semi-analytical solutions for the longitudinal waves nonlinear propagation and nonlinear damage interaction in a damaged beam. Furthermore, those solutions can be decomposed onto an appropriate modal basis for simulation purposes. We have shown through a simulation example that both proposed approaches for simulations gave qualitatively and quantitatively similar results than a state-of-the-art finite element method. Furthermore, a method for estimating the stiffness characteristic was proposed and shown to be robust when the damage respects the assumption of

polynomial approximation. The advantages and drawbacks of this framework as well as its practical usefulness for SHM purposes have been discussed in details. Such a framework thus paves the road for several perspectives from both the theoretical and applied point of view.

Acknowledgements

This work has received funding from the European Union's Horizon 2020 research and innovation program under the REMAP project (grant agreement number 769288).

A Computation of semi-analytical solution

A.1 Dynamic part ($s \neq 0$)

Equation (20-1) admits general solutions of the form

$$U_n(x,s) = \begin{cases} A_l(s)\cosh\Big(\sigma(s)x\Big) + B_l(s)\sinh\Big(\sigma(s)x\Big) + \dfrac{1}{\sigma(s)}\displaystyle\int_0^x G_n(\xi,s)\sinh\Big(\sigma(s)(\xi-x)\Big)d\xi & \text{for } x\in\Omega_l\,, \\ A_r(s)\cosh\Big(\sigma(s)\,(L-x)\Big) + B_r(s)\sinh\Big(\sigma(s)\,(L-x)\Big) & \\ \quad + \dfrac{1}{\sigma(s)}\displaystyle\int_L^x G_n(\xi,s)\sinh\Big(\sigma(s)(\xi-x)\Big)d\xi & \text{for } x\in\Omega_r\,. \end{cases}$$

Boundary conditions (20-2) at $x = 0$ and (20-3) at $x = L$ imposes

$$U_n(x,s) = \begin{cases} B_l(s)\sinh\Big(\sigma(s)x\Big) + \dfrac{1}{\sigma(s)}\displaystyle\int_0^x G_n(\xi,s)\sinh\Big(\sigma(s)(\xi-x)\Big)d\xi & \text{for } x\in\Omega_l\,, \\ B_r(s)\sinh\Big(\sigma(s)\,(L-x)\Big) + \dfrac{1}{\sigma(s)}\displaystyle\int_L^x G_n(\xi,s)\sinh\Big(\sigma(s)(\xi-x)\Big)d\xi & \text{for } x\in\Omega_r\,. \end{cases} \tag{43}$$

Damage condition (20-4) at $x = d$ imposes

$$B_l(s) = -B_r(s)\frac{\cosh\left(\sigma(s)\delta\right)}{\cosh\left(\sigma(s)d\right)} + \frac{1}{\sigma(s)}\int_0^L G_n(\xi,s)\frac{\cosh\left(\sigma(s)(\xi-d)\right)}{\cosh\left(\sigma(s)d\right)}d\xi\,.$$

Damage condition (20-5) at $x = d$ then leads to

$$\begin{aligned} B_r(s) = {} & \frac{F_0}{Q\,(s)}\int_d^L G_n(\xi,s)\cosh\Big(\sigma(s)(\xi-d)\Big)\cosh\Big(\sigma(s)d\Big)d\xi \\ & + \frac{K_1}{\sigma(s)Q\,(s)}\int_0^L G_n(\xi,s)\sinh\Big(\sigma(s)\xi\Big)d\xi - \frac{R_n\,(s)}{Q\,(s)}\cosh\Big(\sigma(s)d\Big)\,, \end{aligned} \tag{44}$$

and so

$$B_l(s) = \frac{F_0}{Q\,(s)} \int_0^d G_n(\xi, s) \cosh\Big(\sigma(s)\delta\Big) \cosh\Big(\sigma(s)(\xi - d)\Big) d\xi \\ + \frac{K_1}{\sigma(s) Q\,(s)} \int_0^L G_n(\xi, s) \sinh\Big(\sigma(s)\,(L - \xi)\Big) d\xi + \frac{R_n\,(s)}{Q\,(s)} \cosh\Big(\sigma(s)\delta\Big) \tag{45}$$

Incorporating (45) and (44) into (43) leads to the final result (21).

A.2 Static part ($s = 0$)

Equation (20-1) admits general solutions of the form

$$U_n\,(x, 0) = \begin{cases} A_l + B_l x + \displaystyle\int_0^x G_n\,(\xi, 0)\,(\xi - x)\, d\xi & \text{for } x \in \Omega_l\,, \\ A_r + B_r\,(L - x) + \displaystyle\int_L^x G_n\,(\xi, 0)\,(\xi - x)\, d\xi & \text{for } x \in \Omega_r\,. \end{cases} \tag{46}$$

Boundary conditions (20-2) at $x = 0$ and (20-4) at $x = L$ imposes

$$U_n\,(x, 0) = \begin{cases} B_l x + \displaystyle\int_0^x G_n\,(\xi, 0)\,(\xi - x)\, d\xi & \text{for } x \in \Omega_l\,, \\ B_r\,(L - x) + \displaystyle\int_L^x G_n\,(\xi, 0)\,(\xi - x)\, d\xi & \text{for } x \in \Omega_r\,. \end{cases} \tag{47}$$

Damage condition (20-4) at $x = d$ imposes

$$B_l = -B_r + \int_0^L G_n\,(\xi, 0)\, d\xi\,. \tag{48}$$

Damage condition (20-5) at $x = d$ then leads to

$$B_r = \frac{F_0}{F_0 + K_1 L} \int_d^L G_n\,(\xi, 0)\, d\xi + \frac{K_1}{F_0 + K_1 L} \int_0^L G_n\,(\xi, 0)\, \xi d\xi - \frac{R_n\,(0)}{F_0 + K_1 L}\,, \tag{49}$$

and so

$$B_l = \frac{F_0}{F_0 + K_1 L} \int_0^d G_n\,(\xi, 0)\, d\xi + \frac{K_1}{F_0 + K_1 L} \int_0^L G_n\,(\xi, 0)\,(L - \xi)\, d\xi + \frac{R_n\,(0)}{F_0 + K_1 L}\,. \tag{50}$$

Incorporating (50) and (49) into (47) leads to the final result (23).

B Computation of modal solution

B.1 Determination of modal shapes

We search an orthonormal family of modes ϕ such that they all respect

$$\begin{cases} \phi''(x) + \lambda^2 \phi(x) = 0 & \text{for } x \in \Omega_l \cup \Omega_r \\ \phi(0) = 0 \\ \phi(L) = 0 \\ \phi'(d^-) = \phi'(d^+) = \phi'(d) \\ F_0 \phi'(d) - K_1 \phi(d^+) + K_1 \phi(d^-) = 0 \\ \int_0^L \phi^2(x)\, dx = 1 \end{cases} \tag{51}$$

Equation (51-1) admits general solutions of the form

$$\phi(x) = \begin{cases} A_l \cos(\lambda x) + B_l \sin(\lambda x) & \text{for } x \in \Omega_l\,, \\ A_r \cos\Big(\lambda(L-x)\Big) + B_r \sin\Big(\lambda(L-x)\Big) & \text{for } x \in \Omega_r\,. \end{cases} \tag{52}$$

Boundary conditions (51-2) at $x = 0$ and (51-3) at $x = L$ imposes

$$A_l = 0\,, \tag{53}$$
$$A_r = 0\,. \tag{54}$$

Then damage condition (51-4) at $x = d$ imposes

$$B_l \cos(\lambda d) = -B_r \cos(\lambda \delta)\,, \tag{55}$$

and damage condition (51-5) at $x = d$ imposes

$$-F_0 B_r \lambda \cos(\lambda\delta) - K_1 B_r \sin(\lambda\delta) + K_1 B_l \sin(\lambda d) = 0\,. \tag{56}$$

Furthermore, normality condition (51-6) imposes

$$B_l^2 \left(\frac{d}{2} - \frac{\sin(2\lambda d)}{4\lambda}\right) + B_r^2 \left(\frac{\delta}{2} - \frac{\sin(2\lambda\delta)}{4\lambda}\right) = 1\,. \tag{57}$$

In order to use relation (55), consider two different cases.

General case:
Suppose $\cos(\lambda d) \neq 0$. Then (55) gives

$$B_l = -B_r \frac{\cos(\lambda\delta)}{\cos(\lambda d)}\,, \tag{58}$$

and equation (56) thus shows that λ must be solution of the transcendental equation

$$F_0 + K_1 \left(\frac{\operatorname{sinc}(\lambda\delta)}{\cos(\lambda\delta)} + \frac{\operatorname{sinc}(\lambda d)}{\cos(\lambda d)}\right) = 0\,. \tag{59}$$

Normality condition (57) becomes

$$B_r = \sqrt{\frac{2\cos(\lambda d)^2}{d\cos(\lambda\delta)^2\Big(1-\mathrm{sinc}(2\lambda d)\Big)+\delta\cos(\lambda d)^2\Big(1-\mathrm{sinc}(2\lambda\delta)\Big)}}\,, \tag{60}$$

and thus

$$B_l = -\sqrt{\frac{2\cos(\lambda\delta)^2}{d\cos(\lambda\delta)^2\Big(1-\mathrm{sinc}(2\lambda d)\Big)+\delta\cos(\lambda d)^2\Big(1-\mathrm{sinc}(2\lambda\delta)\Big)}}\,. \tag{61}$$

Particular case:

Now suppose $\cos(\lambda d) = 0$. Then (55) gives

$$\cos(\lambda\delta) = 0 \tag{62}$$

in order for B_r to not be equal to 0. Therefore wavenumber λ follows

$$\lambda = \frac{(p+1/2)\pi}{d} \text{ for } p \in \mathbb{N}\,, \tag{63}$$

and

$$\lambda = \frac{(q+1/2)\pi}{\delta} \text{ for } q \in \mathbb{N}\,. \tag{64}$$

Thus

$$\begin{aligned}\lambda d + \lambda\delta &= \frac{(p+1/2)\,\pi}{d}d + \frac{(q+1/2)\,\pi}{\delta}\delta \\ \Leftrightarrow \lambda L &= (p+1/2)\,\pi + (q+1/2)\,\pi \\ \Leftrightarrow \lambda &= \frac{(p+q+1)\,\pi}{L}\,.\end{aligned}$$

It is then possible to show that

$$\phi(x) = B_l \sin(\lambda x) \tag{65}$$

for $x \in [0, L]$. Normality condition (51-6) thus becomes

$$B_l = \sqrt{\frac{2}{L}}\,. \tag{66}$$

B.2 Modes orthogonality

For any $(p, q) \in \mathbb{N}^2$, it is possible to decompose the scalar product between modes ϕ_p and ϕ_q according to the left and right parts of the damaged beams as follows:

$$\langle\phi_p, \phi_q\rangle = \langle\phi_p, \phi_q\rangle_l + \langle\phi_p, \phi_q\rangle_r\,. \tag{67}$$

Because both modes ϕ_p and ϕ_q follow the differential equation (51-1) describing longitudinal waves propagation with their respective wavelengths λ_p and λ_q, the following equations can be obtained:

$$\langle\phi_p'', \phi_q\rangle + \lambda_p^2\langle\phi_p, \phi_q\rangle = 0\,, \tag{68}$$

$$\langle\phi_q'', \phi_p\rangle + \lambda_q^2\langle\phi_q, \phi_p\rangle = 0\,. \tag{69}$$

By combining both equations, it is possible to write that:

$$(\lambda_p^2 - \lambda_q^2)\langle\phi_p, \phi_q\rangle = \langle\phi_p'', \phi_q\rangle - \langle\phi_q'', \phi_p\rangle \tag{70}$$

Through double part integration, one then obtains:

$$\langle\phi_p'', \phi_q\rangle_l = \phi_p'(d)\phi_q(d^-) - \phi_q'(d)\phi_p(d^-) + \langle\phi_q'', \phi_p\rangle_l \,, \tag{71}$$

$$\langle\phi_p'', \phi_q\rangle_r = -\phi_p'(d)\phi_q(d^+) + \phi_q'(d)\phi_p(d^+) + \langle\phi_q'', \phi_p\rangle_r \,. \tag{72}$$

Then, it is possible to write:

$$\langle\phi_p'', \phi_q\rangle - \langle\phi_q'', \phi_p\rangle = \phi_p'(d)\Big(\phi_q(d^-) - \phi_q(d^+)\Big) - \phi_q'(d)\Big(\phi_p(d^-) - \phi_p(d^+)\Big) \tag{73}$$

And given that according to equation (51-5) for any mode ϕ satisfying Eqs. (51), the following relations holds:

$$\phi(d^+) - \phi(d^-) = \frac{F_0}{K_1}\phi'(d) \tag{74}$$

It can then be concluded that if $p \neq q$ and thus $\lambda_p \neq \lambda_q$ then:

$$\langle\phi_p, \phi_q\rangle = 0 \tag{75}$$

which demonstrates modes orthogonality.

B.3 Computation of modal solution

Problem (15) contains one inhomogeneous boundary condition (i.e. $\mathcal{D}_x\left[u_n\right](t) = u_n\left(t\right)$) that cannot be modelled using the modal shapes given by (51). Therefore the modal solution will be of the form

$$u_n\left(x,t\right) = u_n^{(\mathrm{bc})}\left(x,t\right) + \sum_{p=1}^{+\infty} \phi_p\left(x\right) u_{n,p}\left(t\right) \,, \tag{76}$$

where $u_n^{(bc)}$ is solution of the boundary problem but considering no propagation, i.e.

$$\begin{cases} u_n^{(bc)}\left(0,t\right) = 0 \\ u_n^{(bc)}\left(L,t\right) = 0 \\ \partial_x u_n^{(bc)}\left(d^-,t\right) = \partial_x u_n^{(bc)}\left(d^+,t\right) \\ \mathcal{D}_x\left[u_n^{(bc)}\right](t) = r_n\left(t\right) \end{cases} \tag{77}$$

and where $u_{n,p}$ is the time evolution of modal shape ϕ_p. In order for u_n to follow the differential equation (15) (i.e. in order to have $\mathcal{L}_{x,t}\left[u_n\right](x,t) = g_n\left(x,t\right)$), we can show, using linearity of differential operator $\mathcal{L}_{x,t}$ and the orthonormality of modes ϕ, that we must have, for all mode number p,

$$\mathcal{L}_{x,t}\left[\langle u_n^{(\mathrm{bc})}, \phi_p\rangle\right](t) + \frac{1}{c_L^2}\ddot{u}_{n,p}\left(t\right) + \frac{\gamma}{F_0}\dot{u}_{n,p}\left(t\right) + \lambda_p^2 u_{n,p}\left(t\right) = \langle g_n, \phi_p\rangle\left(t\right) \,, \tag{78}$$

where the notation $\langle a, b\rangle$ corresponds to the spatial scalar product between a and b (see Equation (32)).
The solution of the boundary problem $u_n^{(\mathrm{bc})}$ is given by

$$u_n^{(2)}(x,t) = h(x)\, r_n(t)\ , \tag{79}$$

where h follows the equations

$$\begin{cases} h(0) = 0 \\ h(L) = 0 \\ \partial_x h(d^-) = \partial_x h(d^+) \\ \mathcal{D}_x[h] = 1 \end{cases} \tag{80}$$

We take

$$h(x) = \begin{cases} \dfrac{x}{F_0 + K_1 L} & \text{for } x \in \Omega_l\ , \\ -\dfrac{(L-x)}{F_0 + K_1 L} & \text{for } x \in \Omega_r\ . \end{cases} \tag{81}$$

Therefore

$$\mathcal{L}_{x,t}\left[u_n^{(\mathrm{bc})}\right](x,t) = h(x)\left(\frac{\gamma}{F_0}\dot{r}_n(t) + \frac{1}{c_L^2}\ddot{r}_n(t)\right), \tag{82}$$

which leads to the ordinary differential equation (31) followed by the time evolutions $u_{n,p}$.
Furthermore, scalar product $\langle h, \phi_p\rangle$ is given by

$$\langle h, \phi_p\rangle = \frac{1}{F_0 + K_1 L} \times \frac{A_p}{\lambda_p^2}\Big(\lambda_p (L-2d)\cos(\lambda_p \delta) - \tan(\lambda_p L)\Big) \tag{83}$$

in the general case (i.e. when ϕ_p follows (24)), and

$$\langle h, \phi_p\rangle = 0 \tag{84}$$

in the particular case (i.e. when ϕ_p follows (28)),

References

[1] Anders Rytter. *Vibrational Based Inspection of Civil Engineering Structures*. PhD thesis, Denmark, 1993.

[2] Charles R Farrar and Keith Worden. An introduction to structural health monitoring. *Philosophical Transactions of the Royal Society A: Mathematical, Physical and Engineering Sciences*, 365(1851):303–315, 2007.

[3] Keith Worden, Charles R Farrar, Graeme Manson, and Gyuhae Park. The fundamental axioms of structural health monitoring. *Proceedings of the Royal Society A: Mathematical, Physical and Engineering Sciences*, 463(2082):1639–1664, 2007.

[4] Zhongqing Su, Lin Ye, and Ye Lu. Guided lamb waves for identification of damage in composite structures: A review. *Journal of sound and vibration*, 295(3-5):753–780, 2006.

[5] Zhongqing Su and Lin Ye. *Identification of damage using Lamb waves: from fundamentals to applications*, volume 48. Springer Science & Business Media, 2009.

[6] Mira Mitra and S Gopalakrishnan. Guided wave based structural health monitoring: A review. *Smart Materials and Structures*, 25(5):053001, 2016.

[7] Nazih Mechbal, Juan Sebastian Uribe, and Marc Rébillat. A probabilistic multi-class classifier for structural health monitoring. *Mechanical Systems and Signal Processing*, 60:106–123, 2015.

[8] Claude Fendzi, Marc Rebillat, Nazih Mechbal, Mikhail Guskov, and Gérard Coffignal. A data-driven temperature compensation approach for structural health monitoring using lamb waves. *Structural Health Monitoring*, 15(5):525–540, 2016.

[9] Claude Fendzi, Nazih Mechbal, Marc Rebillat, Mikhail Guskov, and G Coffignal. A general bayesian framework for ellipse-based and hyperbola-based damage localization in anisotropic composite plates. *Journal of Intelligent Material Systems and Structures*, 27(3):350–374, 2016.

[10] Marc Rébillat, Ouadie Hmad, Farid Kadri, and Nazih Mechbal. Peaks over threshold–based detector design for structural health monitoring: Application to aerospace structures. *Structural Health Monitoring*, 17(1):91–107, 2018.

[11] Marc Rébillat and Nazih Mechbal. Damage localization in geometrically complex aeronautic structures using canonical polyadic decomposition of lamb wave difference signal tensors. *Structural Health Monitoring*, 19(1):305–321, 2020.

[12] K.-Y. Jhang. Nonlinear ultrasonic techniques for nondestructive assessment of micro damage in material: a review. *International journal of precision engineering and manufacturing*, 10(1):123–135, 2009.

[13] A. Novak, M. Bentahar, V. Tournat, R. El Guerjouma, and L. Simon. Nonlinear acoustic characterization of micro-damaged materials through higher harmonic resonance analysis. *NDT & E International*, 45(1):1–8, January 2012.

[14] F Ciampa, E Onder, E Barbieri, and M Meo. Detection and modelling of nonlinear elastic response in damaged composite structures. *Journal of Nondestructive Evaluation*, 33(4):515–521, 2014.

[15] Francesco Ciampa, Ettore Barbieri, and Michele Meo. Modelling of multiscale nonlinear interaction of elastic waves with three-dimensional cracks. *The Journal of the Acoustical Society of America*, 135(6):3209–3220, 2014.

[16] Ming Hong, Zhongqing Su, Qiang Wang, Li Cheng, and Xinlin Qing. Modeling nonlinearities of ultrasonic waves for fatigue damage characterization: Theory, simulation, and experimental validation. *Ultrasonics*, 54(3):770–778, 2014.

[17] N. P. Yelve, M. Mitra, and P.M. Mujumdar. Higher harmonics induced in lamb wave due to partial debonding of piezoelectric wafer transducers. {*NDT*} *& E International*, 63:21 – 27, 2014.

[18] Reza Soleimanpour, Ching-Tai Ng, and Chun H Wang. Higher harmonic generation of guided waves at delaminations in laminated composite beams. *Structural Health Monitoring*, 16(4):400–417, 2017.

[19] Yi Yang, Ching-Tai Ng, Andrei Kotousov, Hoon Sohn, and Hyung Jin Lim. Second harmonic generation at fatigue cracks by low-frequency lamb waves: experimental and numerical studies. *Mechanical Systems and Signal Processing*, 99:760–773, 2018.

[20] Vera Marcantonio, Danilo Monarca, Andrea Colantoni, and Massimo Cecchini. Ultrasonic waves for materials evaluation in fatigue, thermal and corrosion damage: A review. *Mechanical Systems and Signal Processing*, 120:32 – 42, 2019.

[21] Gaetan Kerschen, Keith Worden, Alexander F Vakakis, and Jean-Claude Golinval. Past, present and future of nonlinear system identification in structural dynamics. *Mechanical systems and signal processing*, 20(3):505–592, 2006.

[22] Jean-Philippe Noël and Gaëtan Kerschen. Nonlinear system identification in structural dynamics: 10 more years of progress. *Mechanical Systems and Signal Processing*, 83:2–35, 2017.

[23] Charles R Farrar, Keith Worden, Michael D Todd, Gyuhae Park, Jonathon Nichols, Douglas E Adams, Matthew T Bement, and Kevin Farinholt. Nonlinear system identification for damage detection. Technical report, Los Alamos National Laboratory (LANL), Los Alamos, NM, 2007.

[24] Keith Worden, Charles R Farrar, Jonathan Haywood, and Michael Todd. A review of nonlinear dynamics applications to structural health monitoring. *Structural Control and Health Monitoring: The Official Journal of the International Association for Structural Control and Monitoring and of the European Association for the Control of Structures*, 15(4):540–567, 2008.

[25] Jonathan M Nichols and Michael D Todd. Nonlinear features for shm applications. *Encyclopedia of structural health monitoring*, 2009.

[26] Timothy J Johnson and Douglas E Adams. Transmissibility as a differential indicator of structural damage. *Journal of Vibration and Acoustics*, 124(4):634–641, 2002.

[27] M. Haroon and D. E. Adams. Time and frequency domain nonlinear system characterization for mechanical fault identification. *Nonlinear Dynamics*, 50(3):387–408, November 2007.

[28] Wang-Ji Yan, Meng-Yun Zhao, Qian Sun, and Wei-Xin Ren. Transmissibility-based system identification for structural health monitoring: Fundamentals, approaches, and applications. *Mechanical Systems and Signal Processing*, 117:453–482, 2019.

[29] ZQ Lang and ZK Peng. A novel approach for nonlinearity detection in vibrating systems. *Journal of Sound and Vibration*, 314(3-5):603–615, 2008.

[30] Zi-Qiang Lang, Gyuhae Park, Charles R Farrar, Michael D Todd, Zhu Mao, L Zhao, and Keith Worden. Transmissibility of non-linear output frequency response functions with application in detection and location of damage in mdof structural systems. *International Journal of Non-Linear Mechanics*, 46(6):841–853, 2011.

[31] CM Cheng, ZK Peng, WM Zhang, and Guang Meng. Volterra-series-based nonlinear system modeling and its engineering applications: A state-of-the-art review. *Mechanical Systems and Signal Processing*, 87:340–364, 2017.

[32] D. E. Adams and C. R. Farrar. Application of frequency domain ARX features for linear and nonlinear structural damage identification. *Smart Nondestructive Evaluation for Health Monitoring of Structural and Biological Systems*, 4702:134–147, 2002.

[33] Douglas E. Adams and Charles R. Farrar. Classifying linear and nonlinear structural damage using frequency domain ARX models. *Structural Health Monitoring - An International Journal*, 1(2):185–201, 2002.

[34] L. Bornn, C. R. Farrar, G. Park, and K. Farinholt. Structural health monitoring with autoregressive support vector machines. *Journal of Vibration and Acoustics-transactions of the Asme*, 131(2):021004, April 2009.

[35] L. Bornn, C. R. Farrar, and G. Park. Damage detection in initially nonlinear systems. *International Journal of Engineering Science*, 48(10):909–920, October 2010.

[36] Sidney Bruce Shiki, Vicente Lopes, and Samuel Da Silva. Damage detection in nonlinear structures using discrete-time volterra series. In *Key Engineering Materials*, volume 569, pages 876–883. Trans Tech Publ, 2013.

[37] CM Cheng, ZK Peng, XJ Dong, WM Zhang, and Guang Meng. A novel damage detection approach by using volterra kernel functions based analysis. *Journal of the Franklin Institute*, 352(8):3098–3112, 2015.

[38] Sidney B Shiki, Samuel da Silva, and Michael D Todd. On the application of discrete-time volterra series for the damage detection problem in initially nonlinear systems. *Structural Health Monitoring*, 16(1):62–78, 2017.

[39] Marc Rébillat, Rafik Hajrya, and Nazih Mechbal. Nonlinear structural damage detection based on cascade of hammerstein models. *Mechanical Systems and Signal Processing*, 48(1-2):247–259, 2014.

[40] Meriem Ghrib, Marc Rébillat, Guillaume Vermot des Roches, and Nazih Mechbal. Automatic damage type classification and severity quantification using signal based and nonlinear model based damage sensitive features. *Journal of Process Control*, 83:136–146, 2019.

[41] Luis GG Villani, Samuel Da Silva, and Americo Cunha Jr. Damage detection in uncertain nonlinear systems based on stochastic volterra series. *Mechanical Systems and Signal Processing*, 125:288–310, 2019.

[42] Luis GG Villani, Samuel Da Silva, Americo Cunha Jr, and Michael D Todd. Damage detection in an uncertain nonlinear beam based on stochastic volterra series: an experimental application. *Mechanical Systems and Signal Processing*, 128:463–478, 2019.

[43] Luis GG Villani, Samuel da Silva, Americo Cunha, and Michael D Todd. On the detection of a nonlinear damage in an uncertain nonlinear beam using stochastic volterra series. *Structural Health Monitoring*, 19(4):1137–1150, 2020.

[44] J Prawin and A Rama Mohan Rao. Nonlinear structural damage detection based on adaptive volterra filter model. *International Journal of Structural Stability and Dynamics*, 18(02):1871003, 2018.

[45] J Prawin and A Rama Mohan Rao. Extraction of opening and closing states of cracked structure using adaptive volterra filter model. *Procedia Structural Integrity*, 14:234–241, 2019.

[46] Wilson John Rugh. *Nonlinear system theory.* Johns Hopkins University Press Baltimore, 1981.

[47] Stephen Boyd and Leon O. Chua. Fading memory and the problem of approximating nonlinear operators with Volterra series. *IEEE Transactions on Circuits and Systems*, 32(11):1150–1161, 1985.

[48] Han-Xiong Li, Chenkun Qi, and Yongguang Yu. A spatio-temporal volterra modeling approach for a class of distributed industrial processes. *Journal of Process Control*, 19(7):1126–1142, 2009.

[49] David Roze and Thomas Hélie. Introducing a Green–Volterra series formalism to solve weakly nonlinear boundary problems: Application to Kirchhoff's string. *Journal of Sound and Vibration*, 333(7):2073–2086, 2014.

[50] Emmanuel Lizé, Marc Rébillat, Nazih Mechbal, and Christian Bolzmacher. Optimal dual-pzt sizing and network design for baseline-free shm of complex anisotropic composite structures. *Smart Materials and Structures*, 27(11):115018, 2018.

[51] Shuanglin Guo, Marc Rebillat, and Nazih Mechbal. Dichotomy property of dispersion equation of guided waves propagating in anisotropic composite plates. *Mechanical Systems and Signal Processing*, 164:108212, 2022.

[52] Dariusz Broda, W.J. Staszewski, A. Martowicz, T. Uhl, and V.V. Silberschmidt. Modelling of nonlinear crack–wave interactions for damage detection based on ultrasound—a review. *Journal of Sound and Vibration*, 333(4):1097–1118, 2014.

[53] Zi Qiang Lang, Stephen A. Billings, R. Yue, and J. Li. Output frequency response function of nonlinear Volterra systems. *Automatica*, 43(5):805–816, 2007.

[54] B. Zhang and S.A. Billings. Volterra series truncation and kernel estimation of nonlinear systems in the frequency domain. *Mechanical Systems and Signal Processing*, 84:39–57, 2017.

[55] E. Balmes. *Structural Dynamics Toolbox (for use with MATLAB)*. www.sdtools.com.

[56] Stephen Boyd, YS Tang, and Leon Chua. Measuring volterra kernels. *IEEE transactions on circuits and systems*, 30(8):571–577, 1983.

[57] Damien Bouvier, Thomas Hélie, and David Roze. Nonlinear homogeneous order separation for volterra series identification. In *20th International Conference on Digital Audio Effects*, 2017.

[58] Damien Bouvier, Thomas Hélie, and David Roze. Phase-based order separation for volterra series identification. *International Journal of Control*, 0(0):1–11, 2019.

[59] Johan Schoukens and Lennart Ljung. Nonlinear system identification: A user-oriented road map. *IEEE Control Systems Magazine*, 39(6):28–99, 2019.

[60] Wieslaw Staszewski, Geoffrey Tomlinson, Christian Boller, and Geof Tomlinson. *Health monitoring of aerospace structures*. Wiley Online Library, 2004.

[61] Stephen Boyd, Leon O Chua, and Charles A Desoer. Analytical foundations of Volterra series. *IMA Journal of Mathematical Control and Information*, 1(3):243–282, 1984.

[62] Stephen P. Boyd. *Volterra series: Engineering fundamentals*. PhD thesis, University of California, Berkeley, 1985.

[63] Matthieu Gresil and Victor Giurgiutiu. Prediction of attenuated guided waves propagation in carbon fiber composites using rayleigh damping model. *Journal of Intelligent Material Systems and Structures*, 26(16):2151–2169, 2015.

[64] Christoph Heinze, Sascha Duczek, and Michael Sinapius. A minimal model for fast approximation of lamb wave propagation in complex aircraft parts. In *Lamb-Wave Based Structural Health Monitoring in Polymer Composites*, pages 241–261. Springer, 2018.

[65] J. C. P. Mckeon and M. K. Hinders. Lamb wave scattering from a through hole. *Journal of Sound and Vibration*, 224(5):843–862, July 1999.

[66] Tomas Grahn. Lamb wave scattering from a circular partly through-thickness hole in a plate. *Wave Motion*, 37(1):63–80, January 2003.

[67] Chun H. Wang and Fu-Kuo Chang. Scattering of plate waves by a cylindrical inhomogeneity. *Journal of Sound and Vibration*, 282(1):429–451, April 2005.

[68] Nassim Benbara, Marc Rebillat, and Nazih Mechbal. Bending waves focusing in arbitrary shaped plate-like structures: Application to spatial audio in cars. *Journal of Sound and Vibration*, 487:115587, 2020.

[69] Amirhossein Rahbari, Marc Rébillat, Nazih Mechbal, and Stephane Canu. Unsupervised damage clustering in complex aeronautical composite structures monitored by lamb waves: An inductive approach. *Engineering Applications of Artificial Intelligence*, 97:104099, 2021.

[70] Wiesław M Ostachowicz and Marek Krawczuk. On modelling of structural stiffness loss due to damage. In *Key Engineering Materials*, volume 204, pages 185–200. Trans Tech Publ, 2001.

[71] Vincentius Ewald, Roger M Groves, and Rinze Benedictus. Deepshm: a deep learning approach for structural health monitoring based on guided lamb wave technique. In *Sensors and Smart Structures Technologies for Civil, Mechanical, and Aerospace Systems 2019*, volume 10970, page 109700H. International Society for Optics and Photonics, 2019.

[72] Vincentius Ewald, Ramanan Sridaran Venkat, Aadhik Asokkumar, Rinze Benedictus, Christian Boller, and Roger M Groves. Perception modelling by invariant representation of deep learning for automated structural diagnostic in aircraft maintenance: A study case using deepshm. *Mechanical Systems and Signal Processing*, 165:108153, 2022.